Scalable Solvers of Random Quadratic Equations via Stochastic Truncated Amplitude Flow

Gang Wang, *Student Member, IEEE*, Georgios B. Giannakis, *Fellow, IEEE*, and Jie Chen, *Senior Member, IEEE*

Abstract—**A novel approach termed *stochastic truncated amplitude flow* (STAF) is developed to reconstruct an unknown n-dimensional real-/complex-valued signal $\boldsymbol{x}$ from m 'phaseless' quadratic equations of the form $\psi_i = |\langle \boldsymbol{a}_i, \boldsymbol{x}\rangle|$. This problem, also known as phase retrieval from magnitude-only information, is *NP-hard* in general. Adopting an amplitude-based nonconvex formulation, STAF leads to an iterative solver comprising two stages: s1) Orthogonality-promoting initialization through a stochastic variance reduced gradient algorithm; and, s2) A series of iterative refinements of the initialization using stochastic truncated gradient iterations. Both stages involve a single equation per iteration, thus rendering STAF a simple, scalable, and fast approach amenable to large-scale implementations that is useful when n is large. When $\{\boldsymbol{a}_i\}_{i=1}^m$ are independent Gaussian, STAF provably recovers exactly any $\boldsymbol{x} \in \mathbb{R}^n$ exponentially fast based on order of n quadratic equations. STAF is also robust in the presence of additive noise of bounded support. Simulated tests involving real Gaussian $\{\boldsymbol{a}_i\}$ vectors demonstrate that STAF empirically reconstructs any $\boldsymbol{x} \in \mathbb{R}^n$ exactly from about $2.3n$ magnitude-only measurements, outperforming state-of-the-art approaches and narrowing the gap from the information-theoretic number of equations $m = 2n-1$. Extensive experiments using synthetic data and real images corroborate markedly improved performance of STAF over existing alternatives.**

Index terms— Nonconvex optimization, phase retrieval, variance reduction, Kaczmarz algorithm.

I. INTRODUCTION

Consider the fundamental problem of reconstructing a general signal vector from magnitude-only measurements, e.g., the magnitude of the Fourier transform or any linear transform of the signal. This problem, also known as *phase retrieval* [1], arises in many fields of science and engineering ranging from X-ray crystallography [2], optics [3], as well as coherent diffraction imaging [4]. In such settings, due to the physical limitations of optical detectors such as photosensitive films, charge-coupled device (CCD) cameras, and human eyes, one records only the intensity of light (which describes the absolute counts of photons or electrons that strike the detectors) but loses the phase (where the wave peaks and troughs lie) [5]. It is known that when collecting the diffraction pattern at a large enough distance from the imaging plane, the field is given by the Fourier transform of the image (up to a known phase factor).

Therefore, those optical devices in the far field essentially measure only the squared modulus of the Fourier transform of the object, whereas the phase of the incident light reaching the detector is missing. Nevertheless, very much information is contained in the Fourier phase. It has been well documented that the Fourier phase of an image encodes often more structural information than its Fourier magnitude [6]. Recovering the phase from magnitude-only measurements is thus of paramount practical relevance. Further details concerning recent advances in the theory and practice of phase retrieval can be found in the review [5].

Succinctly stated, the generalized phase retrieval amounts to solving a system of 'phaseless' quadratic equations taking the form

$$\psi_i = |\langle \boldsymbol{a}_i, \boldsymbol{x}\rangle|, \quad 1 \le i \le m \tag{1}$$

where $\boldsymbol{x} \in \mathbb{R}^n$ or $\mathbb{C}^n$ is the wanted unknown, $\boldsymbol{a}_i \in \mathbb{R}^n$ or $\mathbb{C}^n$ are known sensing/feature vectors, and $\boldsymbol{\psi} := [\psi_1 \cdots \psi_m]^{\mathcal{T}}$ is the observed data vector. Equivalently, (1) can also be given in its squared form as $y_i = |\langle \boldsymbol{a}_i, \boldsymbol{x}\rangle|^2$, where $y_i := \psi_i^2$ denotes the intensity or the squared modulus.

In the classical discretized one-dimensional phase retrieval, the amplitude vector $\boldsymbol{\psi}$ corresponds to the m-point (typically, $m = 2n-1$) Fourier transform of the length-n signal $\boldsymbol{x}$ [5]. It has been established using the fundamental theorem of algebra that there is no unique solution in the discretized 1D phase retrieval, even if one fixes trivial ambiguities resulting from operations that preserve Fourier magnitudes, including the global phase shift, conjugate inversion, and spatial shift [7]. In fact, there are up to 2^{n-2} generally distinct signals with common $\boldsymbol{\psi}$ beyond trivial ambiguities [7]. To overcome this ill-posed character of the 1D phase retrieval, different approaches have been suggested. Additional constraints on the unknown signal such as sparsity or non-negativity are enforced in [8], [9], [10], [11], [12], [13], [14], [15]. Other viable options include introducing specific redundancy into measurements leveraging, for example, the short-time Fourier transform [5], [16], or masks [17], or simply assuming random measurements (e.g., random Gaussian $\{\boldsymbol{a}_i\}$ designs) [12], [1], [18], [19]. For analytic concreteness, we will henceforth assume random measurements ψ_i that are collected from the real-valued Gaussian model (1), with independently and identically distributed (i.i.d.) $\boldsymbol{a}_i \sim \mathcal{N}(\boldsymbol{0}, \boldsymbol{I}_n)$. To demonstrate the effectiveness of our proposed algorithm, experimental implementation for the complex-valued Gaussian model with i.i.d. $\boldsymbol{a}_i \sim \mathcal{CN}(\boldsymbol{0}, \boldsymbol{I}_n) := \mathcal{N}(\boldsymbol{0}, \boldsymbol{I}_n/2) + j\mathcal{N}(\boldsymbol{0}, \boldsymbol{I}_n/2)$, and using real images will be included as well.

It has been recently proved that when $m \geq 2n - 1$ or $m \geq 4n - 4$ generic measurements (e.g., from the Gaussian models) are acquired, the system in (1) determines uniquely an n-dimensional real- or complex-valued x (up to a global sign or phase) [20], [21], respectively. In the real case, $m = 2n - 1$ generic measurements are also proved necessary for uniqueness [20]. Postulating existence of a unique solution x, our goal is to devise simple yet effective algorithms amenable to large-scale implementation: i) that provably reconstruct x from a near-optimal number of phaseless quadratic equations as in (1); and ii), that feature in simultaneously low iteration and computational complexities as well as linear convergence rate.

Being a particular instance of nonconvex quadratic programming, the problem of solving quadratic equations subsumes as special cases various classical combinatorial optimization tasks involving Boolean variables (e.g., the *NP-complete* stone problem [22, Section 3.4.1], [18]). Considering for instance the real-valued vectors a_i and x, this problem boils down to assigning signs $s_i = \pm 1$, such that the solution to the system of linear equations $\langle a_i, x \rangle = s_i \sqrt{y_i}$, denoted by z, adheres to the given phaseless equations $|\langle a_i, z \rangle| = \psi_i$, $1 \leq i \leq m$. It is clear that there are a total of 2^m different combinations of $\{s_i\}_{i=1}^m$, whereas only two combinations of these signs leads to x up to a global sign. The complex scenario becomes even more complicated, in which instead of assigning a series of signs $\{s_i\}_{i=1}^m$, one looks for a collection of unimodular complex constants $\{\sigma_i \in \mathbb{C}\}_{i=1}^m$ such that the resulting linear system and the original quadratic system are equivalent. Furthermore, solving quadratic equations has also found applications in estimating the mixture of linear regressions, in which the latent membership variables are viewed as the missing phases [23]. Despite its practical relevance across various science and engineering fields, solving systems of quadratic equations is combinatorial in nature, and *NP-hard* in general.

Notation. Lower- (upper-) case boldface letters denote column vectors (matrices), and calligraphic symbols are reserved for sets. The symbol $\mathcal{T}$ ($\mathcal{H}$) stands for transposition (conjugate transposition), and $\succeq$ for positive semidefinite matrices. For vectors, $\|\cdot\|$ signifies the Euclidean norm, and $\|\cdot\|_1$ denotes the ℓ_1-norm. The symbol $\lceil\cdot\rceil$ is the ceiling operation that returns the smallest integer greater than or equal to the given number. For a given function $g(n)$ of integer $n > 0$, $\Theta(g(n))$ denotes the set of functions $\Theta(g(n)) = \{f(n) :$ there exist positive constants C_1, C_2, and n_0 such that $0 \leq C_1 g(n) \leq f(n) \leq C_2 g(n)$ for all $n \geq n_0\}$; and likewise, $\mathcal{O}(g(n)) = \{f(n) :$ there exist positive constants C and n_0 such that $0 \leq f(n) \leq Cg(n)$ for all $n \geq n_0\}$, and $\Omega(g(n)) = \{f(n) :$ there exist positive constants C and n_0 such that $0 \leq Cg(n) \leq f(n)$ for all $n \geq n_0\}$.

A. Prior Art

Adopting the least-squares criterion (which would coincide with the maximum likelihood one when assuming an additive white Gaussian noise model), the task of tackling the quadratic system in (1) can be reformulated as that of minimizing the following *amplitude-based* empirical loss [9], [12], [19]

$$\underset{z \in \mathbb{C}^n}{\text{minimize}} \quad \frac{1}{2m} \sum_{i=1}^m \left(\psi_i - |a_i^{\mathcal{H}} z| \right)^2 \qquad (2)$$

or, the *intensity-based* one [1]

$$\underset{z \in \mathbb{C}^n}{\text{minimize}} \quad \frac{1}{2m} \sum_{i=1}^m \left(y_i - |a_i^{\mathcal{H}} z|^2 \right)^2 \qquad (3)$$

and its counterpart for Poisson data [18]

$$\underset{z \in \mathbb{C}^n}{\text{minimize}} \quad \frac{1}{2m} \sum_{i=1}^m |a_i^{\mathcal{H}} z|^2 - y_i \log \left(|a_i^{\mathcal{H}} z|^2 \right). \qquad (4)$$

Unfortunately, the three objective functions are nonconvex because of the modulus in (2), or the quadratic terms in (3) and (4). It is well known that nonconvex functions may exhibit many stationary points, and minimizing nonconvex objectives is in general *NP-hard*, and hence computationally intractable [24]. It is worth stressing that it is difficult to establish convergence to a local minimum due to the existence of complicated saddle point structures [24], [25], [26].

Past approaches for solving quadratic equations can be grouped in two categories: convex and nonconvex ones. The nonconvex ones include the 'workhorse' alternating projection algorithms [27], [9], [28], [29], AltMinPhase [12] and TAF [30], [19], [15], [14], trust-region [31] and majorization-minimization [32], [33], as well as the recently proposed Wirtinger-based variants such as (truncated) Wirtinger flow (WF/TWF) [1], [18], [34]. Based on STFT measurements, gradient descent-type algorithms starting with a least-squares initialization provably recover the signal from magnitude-only information under appropriate conditions [16]. Stochastic or incremental counterparts consisting of Kaczmarz and ITWF have been reported too [35], [36]. On the other hand, the convex alternatives typically rely upon the so-called *matrix-lifting* technique to derive semidefinite programming-based solvers such as PhaseLift [37], PhaseCut [38], and CoRK [39]. For the Gaussian model, comparisons between convex and nonconvex solvers in terms of sample complexity and computational complexity to acquire an ϵ-accurate solution are listed in Table I.

B. This Paper

Adopting the amplitude-based nonconvex formulation, this paper puts forth a new algorithm, referred to as *stochastic truncated amplitude flow* (STAF). STAF offers an iterative algorithm that builds upon but considerably broadens the scope of TAF [19]. Specifically, it operates in two stages: Stage one employs a stochastic variance reduced gradient algorithm to obtain an orthogonality-promoting initialization, whereas the second stage applies stochastic truncated amplitude-based iterations to refine the initial estimate. Our approach is shown capable of reconstructing any n-dimensional real-/complex-valued signal x from a nearly minimal number of magnitude-only measurements in linear time. Relative to TAF, the present paper's STAF is well suited for large-scale applications. Besides achieving order-optimal sample and

TABLE I: Comparisons of Different Algorithms

Algorithm	Sample complexity m	Computational complexity
PhaseLift [37]	$\mathcal{O}(n)$	$\mathcal{O}(n^3/\epsilon)$
PhaseCut [38]	$\mathcal{O}(n)$	$\mathcal{O}(n^3/\epsilon)$
AltMinPhase [12]	$\mathcal{O}(n\log n(\log^2 n + \log(1/\epsilon)))$	$\mathcal{O}(n^2\log n(\log^2 n + \log^2(1/\epsilon)))$
WF [1]	$\mathcal{O}(n\log n)$	$\mathcal{O}(n^3\log n\log(1/\epsilon))$
TAF [19], TWF [18], ITWF [36]	$\mathcal{O}(n)$	$\mathcal{O}(n^2\log(1/\epsilon))$
This paper	$\mathcal{O}(n)$	$\mathcal{O}(n^2\log(1/\epsilon))$

computational complexities, STAF enjoys $\mathcal{O}(n)$ per-iteration complexity in both initialization and refinement stages, which not only improves upon state-of-the-art alternatives that can afford $\mathcal{O}(n^2)$, but it is also order optimal. This makes STAF applicable and appealing to common large-scale imaging phase retrieval settings. Although ITWF adopts an incremental gradient method to achieve $\mathcal{O}(n)$ per-iteration complexity at the second stage, its first stage relies on the gradient-type power method of per-iteration complexity $\mathcal{O}(n^2)$ to obtain a truncated spectral initialization [36]. Moreover, as will be demonstrated by our simulated tests, STAF outperforms the state-of-the-art algorithms including TAF, ITWF, and (T)WF on both synthetic data and real images in terms of both exact recovery performance and convergence speed. Specifically for the real-valued Gaussian model, STAF empirically reconstructs any real-valued n-dimensional signal $\boldsymbol{x}$ from a number $m \approx 2.3n$ of magnitude measurements, which is close to the information-theoretic limit of $m = 2n - 1$. In sharp contrast, the existing alternatives such as TAF, ITWF, and (T)WF typically require a few times more measurements to achieve exact recovery. Markedly improved performance is also witnessed for STAF when the complex-valued Gaussian model, and coded diffraction patterns of real images [17], are employed.

Paper outline. The rest of the paper is outlined as follows. Section II first reviews the truncated amplitude flow (TAF) algorithm, and subsequently motivates and derives the two stages of our proposed STAF algorithm. Section III summarizes STAF, and establishes its theoretical performance. Extensive tests comparing STAF with state-of-the-art approaches on both synthetic data and real images are presented in Section IV. Finally, main proofs are given in Section V, and technical details can be found in the Appendix.

II. ALGORITHM: STOCHASTIC TRUNCATED AMPLITUDE FLOW

In this section, TAF is first reviewed, and its limitations for large-scale applications are pointed out. To cope with these limitations, simple, scalable, and fast stochastic gradient descent (SGD)-type algorithms for both the initialization and gradient refinement stages are developed.

To begin with, a number of basic concepts are introduced. If $\boldsymbol{x}$ in the real case solves (1), so does $-\boldsymbol{x}$. In the complex case, the solution set becomes $\{\boldsymbol{x}e^{i\phi}, \forall\phi\}$. This prompts the following definition of the Euclidean distance of any estimate $\boldsymbol{z}$ to the solution set of (1): $\mathrm{dist}(\boldsymbol{z}, \boldsymbol{x}) := \min \|\boldsymbol{z} \pm \boldsymbol{x}\|$ for real-valued signals, and $\mathrm{dist}(\boldsymbol{z}, \boldsymbol{x}) := \mathrm{minimize}_{\phi\in[0,2\pi)}\|\boldsymbol{z} - \boldsymbol{x}e^{i\phi}\|$ for complex ones [1]. Define also the indistinguishable global phase constant in the real case as

$$\phi(\boldsymbol{z}) := \begin{cases} 0, & \|\boldsymbol{z} - \boldsymbol{x}\| \le \|\boldsymbol{z} + \boldsymbol{x}\|, \\ \pi, & \text{otherwise.} \end{cases} \tag{5}$$

Henceforth, letting $\boldsymbol{x}$ be any solution of the given system in (1), we assume that $\phi(\boldsymbol{z}) = 0$; otherwise, $\boldsymbol{z}$ is replaced by $e^{-j\phi(\boldsymbol{z})}\boldsymbol{z}$, but for brevity of exposition, the phase adaptation term $e^{-j\phi(\boldsymbol{z})}$ shall be dropped whenever it is clear from the context.

A. Truncated Amplitude Flow

In this section, the two stages of TAF are outlined [19]. In stage one, TAF employs power iterations to compute an orthogonality-promoting initialization, while the second stage refines the initialization via gradient-type iterations. The orthogonality-promoting initialization builds upon a basic characteristic of high-dimensional spaces, which asserts that high-dimensional random vectors are almost always nearly orthogonal to each other [19]. Its core idea relies on approximating the unknown $\boldsymbol{x}$ by a vector $\boldsymbol{z}_0 \in \mathbb{R}^n$ most orthogonal to a carefully selected subset of design vectors $\{\boldsymbol{a}_i\}_{i\in\mathcal{I}_0}$, with the index set $\mathcal{I}_0 \subseteq [m] := \{1, 2, \ldots, m\}$. It is well known that the geometric relationship between any nonzero vectors $\boldsymbol{p} \in \mathbb{R}^n$ and $\boldsymbol{q} \in \mathbb{R}^n$ can be captured by their squared normalized inner-product defined as $\cos^2\theta := |\langle\boldsymbol{p},\boldsymbol{q}\rangle|^2/(\|\boldsymbol{p}_i\|^2\|\boldsymbol{q}\|^2)$, where $\theta \in [0,\pi]$ signifies the angle between $\boldsymbol{p}$ and $\boldsymbol{q}$. Intuitively, the smaller $\cos^2\theta$ is, the more orthogonal the two vectors are. Assume with no loss of generality that $\|\boldsymbol{x}\| = 1$, which will be justified shortly. Upon obtaining the squared normalized inner-products for all pairs $\{(\boldsymbol{a}_i,\boldsymbol{x})\}_{i=1}^m$, collectively denoted by $\{\cos^2\theta_i\}_{i=1}^m$ with θ_i denoting the angle between $\boldsymbol{a}_i$ and $\boldsymbol{x}$, the orthogonality-promoting initialization constructs $\mathcal{I}_0$ by including the indices of $\boldsymbol{a}_i$'s that produce one of the smallest $|\mathcal{I}_0|$ normalized inner-products. Precisely, $\boldsymbol{z}_0$ can be found by solving [19]

$$\underset{\|\boldsymbol{z}\|=1}{\text{minimize}} \quad \boldsymbol{z}^{\mathcal{T}}\left(\frac{1}{|\mathcal{I}_0|}\sum_{i\in\mathcal{I}_0}\frac{\boldsymbol{a}_i\boldsymbol{a}_i^{\mathcal{T}}}{\|\boldsymbol{a}_i\|^2}\right)\boldsymbol{z} \tag{6}$$

where $|\mathcal{I}_0|$ is on the order of n. To be precise, as shown in [19, Theorem 1], one requires for exact recovery of TAF that $m \ge c_1|\mathcal{I}_0| \ge c_2n$ holds for certain numerical constants $c_1, c_2 > 0$. Solving (6) amounts to finding the smallest eigenvalue and the associated eigenvector of $\boldsymbol{Y}_0 := \frac{1}{|\mathcal{I}_0|}\sum_{i\in\mathcal{I}_0}\frac{\boldsymbol{a}_i\boldsymbol{a}_i^{\mathcal{T}}}{\|\boldsymbol{a}_i\|^2} \succeq \boldsymbol{0}$. Nevertheless, to avoid the $\mathcal{O}(n^3)$ computational complexity of computing the eigenvector associated with the smallest eigenvalue in (6), an application of the standard concentration result $\sum_{i=1}^m \frac{\boldsymbol{a}_i\boldsymbol{a}_i^{\mathcal{T}}}{\|\boldsymbol{a}_i\|^2} \cong \frac{m}{n}\boldsymbol{I}_n$ simplifies that to computing the principal eigenvector of $\overline{\boldsymbol{Y}}_0 := \frac{1}{|\overline{\mathcal{I}}_0|}\sum_{i\in\overline{\mathcal{I}}_0}\frac{\boldsymbol{a}_i\boldsymbol{a}_i^{\mathcal{T}}}{\|\boldsymbol{a}_i\|^2}$, where $\overline{\mathcal{I}}_0$ is

the complement of $\mathcal{I}_0$ in $[m]$. Upon collecting $\{a_i\}_{i \in \bar{\mathcal{I}}_0}$ into an $n \times |\bar{\mathcal{I}}_0|$ data matrix $\boldsymbol{D}$, one can rewrite $\bar{\boldsymbol{Y}}_0 = \boldsymbol{D}\boldsymbol{D}^{\mathcal{T}}$ to arrive at the following principal component analysis (PCA) problem

$$\tilde{\boldsymbol{z}}_0 := \arg \max_{\|\boldsymbol{z}\|=1} \quad \frac{1}{|\bar{\mathcal{I}}_0|} \boldsymbol{z}^{\mathcal{T}} \boldsymbol{D}\boldsymbol{D}^{\mathcal{T}} \boldsymbol{z}. \tag{7}$$

On the other hand, if $\|\boldsymbol{x}\| \neq 1$, the estimate $\tilde{\boldsymbol{z}}_0$ is scaled by $\sqrt{\frac{1}{m}\sum_{i=1}^{m} y_i}$, a norm estimate of $\boldsymbol{x}$ to yield $\boldsymbol{z}_0 := \sqrt{\frac{1}{m}\sum_{i=1}^{m} y_i} \tilde{\boldsymbol{z}}_0$. Further details can be found in [19, Section II.B].

When the signal dimension n is modest, problem (7) can be solved exactly by a full singular value decomposition (SVD) of $\boldsymbol{D}$ [40]. Yet it has running time of $\mathcal{O}(\min\{n^2\bar{\mathcal{I}}_0, n\bar{\mathcal{I}}_0^2\})$ (or simply $\mathcal{O}(n^3)$ because $|\bar{\mathcal{I}}_0|$ is required to be on the order of n), which grows prohibitively in large-scale applications. A common alternative is the power method that is tabulated in Algorithm 1, and was also employed by [19], [1], [18], [36] to find an initialization [40]. Power method, on the other hand, involves a matrix-vector multiplication $\bar{\boldsymbol{Y}}_0\boldsymbol{u}_t$ per iteration, thus incurring per-iteration complexity of $\mathcal{O}(n|\bar{\mathcal{I}}_0|)$ or $\mathcal{O}(n^2)$ by passing through the selected data $\{a_i\}_{i \in \bar{\mathcal{I}}_0}$. Furthermore, to produce an ϵ-accurate solution, it incurs runtime of [40]

$$\mathcal{O}\left(\frac{1}{\delta} n |\bar{\mathcal{I}}_0| \log(1/\epsilon)\right) \tag{8}$$

depending on the eigengap $\delta > 0$, which is defined as the gap between the largest and the second largest eigenvalues of $\bar{\boldsymbol{Y}}_0$ normalized by the largest one [40]. It is clear that when the eigengap δ is small, the runtime of $\mathcal{O}(n|\bar{\mathcal{I}}_0|\log(1/\epsilon)/\delta)$ required by the power method would be equivalent to many passes over the entire data, and this could be prohibitively for large datasets [41]. Hence, the power method may not be appropriate for computing the initialization in large-scale applications, particularly those involving small eigengaps.

Algorithm 1 Power method

1: **Input:** Matrix $\bar{\boldsymbol{Y}}_0 = \boldsymbol{D}\boldsymbol{D}^{\mathcal{T}}$.
2: **Initialize** a unit vector $\boldsymbol{u}_0 \in \mathbb{R}^n$ randomly.
3: **For** $t = 0$ **to** $T - 1$ **do**
$\quad \boldsymbol{u}_{t+1} = \frac{\bar{\boldsymbol{Y}}_0\boldsymbol{u}_t}{\|\bar{\boldsymbol{Y}}_0\boldsymbol{u}_t\|}$.
4: **End for**
5: **Output:** $\tilde{\boldsymbol{z}}_0 = \boldsymbol{u}_T$.

The second stage of TAF relies on truncated gradient iterations of the amplitude-based cost function (4). Specifically, with $t \geq 0$ denoting the iteration number, the truncated gradient stage starts with the initial estimate $\boldsymbol{z}_0$, and operates in the following iterative fashion

$$\boldsymbol{z}_{t+1} = \boldsymbol{z}_t - \frac{\mu}{m} \sum_{i \in \mathcal{I}_{t+1}} \left(\boldsymbol{a}_i^{\mathcal{T}}\boldsymbol{z}_t - \psi_i \frac{\boldsymbol{a}_i^{\mathcal{T}}\boldsymbol{z}_t}{|\boldsymbol{a}_i^{\mathcal{T}}\boldsymbol{z}_t|}\right) \boldsymbol{a}_i, \ \forall t \geq 0 \tag{9}$$

where the index set responsible for the gradient regularization is given as [19]

$$\mathcal{I}_{t+1} := \left\{1 \leq i \leq m \ \middle| \ \frac{|\boldsymbol{a}_i^{\mathcal{T}}\boldsymbol{z}_t|}{|\boldsymbol{a}_i^{\mathcal{T}}\boldsymbol{x}|} \geq \frac{1}{1+\gamma}\right\}, \quad \forall t \geq 0. \tag{10}$$
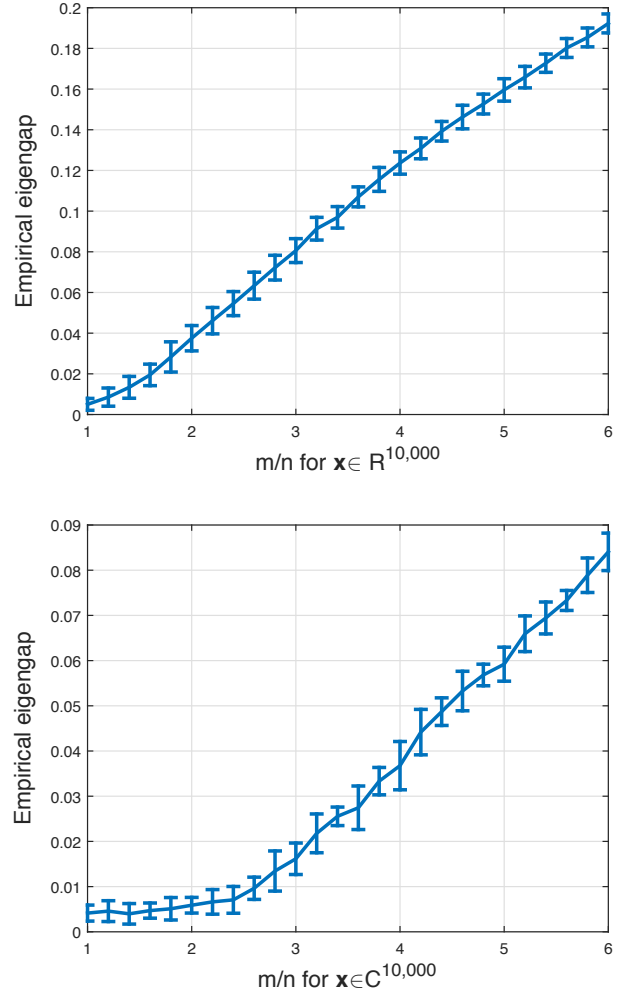

Fig. 1: Rigengaps δ of $\bar{\boldsymbol{Y}}_0 \in \mathbb{R}^{n \times n}$ averaging over 100 Monte Carlo realizations for $n = 10,000$ fixed and m/n varying by 0.2 from 1 to 6. Top: Real-valued Gaussian model with $\boldsymbol{x} \sim \mathcal{N}(\boldsymbol{0}, \boldsymbol{I}_n)$, and $\boldsymbol{a}_i \sim \mathcal{N}(\boldsymbol{0}, \boldsymbol{I}_n)$. Bottom: Complex-valued Gaussian model with $\boldsymbol{x} \sim \mathcal{CN}(\boldsymbol{0}, \boldsymbol{I}_n)$, and $\boldsymbol{a}_i \sim \mathcal{CN}(\boldsymbol{0}, \boldsymbol{I}_n)$.

B. Variance-reducing Orthogonality-promoting Initialization

This section first presents some empirical evidence showing that small eigengaps appear commonly in the orthogonality-promoting initialization approach. Figure 1 plots empirical eigengaps of $\bar{\boldsymbol{Y}}_0 \in \mathbb{R}^{n \times n}$ under the real- and complex-valued Gaussian models over 100 Monte Carlo realizations under default parameters of TAF, where $n = 10,000$ is fixed, and m/n the number of equations and unknowns increases by 0.2 from 1 to 6. As shown in Fig. 1, the eigengaps of $\bar{\boldsymbol{Y}}_0$ resulting from the orthogonality-promoting initialization in [19, Algorithm 1] are rather small particularly for small m/n close to the information limit 2. Using power iterations in Algorithm 1 of runtime $\mathcal{O}(n|\bar{\mathcal{I}}_0|\log(1/\epsilon)/\delta)$ in (8) thus entails many passes over the entire data due to a small eigengap factor of $1/\delta$, which may not perform well in the presence of large dimensions that are common to imaging applications [41]. On the other hand, instead of using the deterministic power

method, stochastic and incremental algorithms have been advocated in [42], [41]. These algorithms perform a much cheaper update per iteration by choosing some $i_t \in \bar{\mathcal{I}}_0$ either uniformly at random or in a cyclic manner, and update the current iterate using only $\boldsymbol{a}_{i_t}$. They are shown to have per-iteration complexity of $\mathcal{O}(n)$, which is very appealing to large-scale applications. Building on recent advances in accelerating stochastic optimization schemes [43], a variance-reducing principal component analysis (VR-PCA) algorithm can be found in [41]. VR-PCA performs cheap stochastic iterations, yet its total runtime is $\mathcal{O}(n(\bar{\mathcal{I}}_0 + 1/\delta^2) \log(1/\epsilon))$ which depends only logarithmically on the solution accuracy $\epsilon > 0$. This is in sharp contrast to the standard SGD variant, whose runtime depends on $1/\epsilon$ due to the large variance of stochastic gradients [42].

For the considered large-scale phase retrieval in most imaging applications, this paper advocates using VR-PCA to solve the orthogonality-promoting initialization problem in (7). We refer to the resulting algorithm as the *variance-reducing orthogonality-promoting initialization* (VR-OPI), which is summarized in Algorithm 2 next. Specifically, VR-OPI is a double-loop algorithm with a single execution of the inner loop referred to as an iteration and one execution of the outer loop referred to as an epoch. In practice, the algorithm consists of S epochs, while each epoch runs T (typically taken to be the data size $|\bar{\mathcal{I}}_0|$) iterations. Note that the full gradient evaluated per execution of the outer loop combined with the stochastic gradients inside the inner loop can be shown capable of reducing the variance of stochastic gradients [43].

Algorithm 2 Variance-reduced orthogonality-promoting initialization (VR-OPI)

1: **Input:** Data matrix $\boldsymbol{D} = \{\boldsymbol{a}_i\}_{i \in \bar{\mathcal{I}}_0}$, step size $\eta = 20/m$, as well as the number of epochs $S = 100$, and the epoch length $T = |\bar{\mathcal{I}}_0|$ (by default).

2: **Initialize** a unit vector $\tilde{\boldsymbol{u}}_0 \in \mathbb{R}^n$ randomly.

3: **For** $s = 0$ **to** $S - 1$ **do**
$\quad \boldsymbol{w} = \frac{1}{|\bar{\mathcal{I}}_0|} \sum_{i \in \bar{\mathcal{I}}_0} \boldsymbol{a}_i(\boldsymbol{a}_i^{\mathcal{T}} \tilde{\boldsymbol{u}}_s)$
$\quad \boldsymbol{u}_1 = \tilde{\boldsymbol{u}}_s$.

4: $\quad$ **For** $t = 0$ **to** $T - 1$ **do**
$\qquad$ Pick $i_t \in \bar{\mathcal{I}}_0$ uniformly at random
$\qquad \boldsymbol{\nu}_{t+1} = \boldsymbol{u}_t + \eta \left[\boldsymbol{a}_{i_t}(\boldsymbol{a}_{i_t}^{\mathcal{T}} \boldsymbol{u}_t - \boldsymbol{a}_{i_t}^{\mathcal{T}} \tilde{\boldsymbol{u}}_s) + \boldsymbol{w} \right]$
$\qquad \boldsymbol{u}_{t+1} = \frac{\boldsymbol{\nu}_{t+1}}{\|\boldsymbol{\nu}_{t+1}\|}$.

5: $\quad$ **End For**
$\quad \tilde{\boldsymbol{u}}_{s+1} = \boldsymbol{u}_T$.

6: **End For**

7: **Output:** $\tilde{\boldsymbol{z}}_0 = \boldsymbol{u}_S$.

The following results adopted from [41, Theorem 1] establish linear convergence rate of VR-OPI.

Proposition 1 ([41]). *Let* $\boldsymbol{v}_1 \in \mathbb{R}^n$ *be an eigenvector of* $\bar{\boldsymbol{Y}}_0$ *associated with the largest eigenvalue* λ_1. *Assume that* $\max_{i \in [m]} \|\boldsymbol{a}_i\|^2 \leq r := 2.3n$ *(which holds with probability at least* $1 - m e^{-n/2}$*), the two largest eigenvalues of* $\bar{\boldsymbol{Y}}_0$ *are* $\lambda_1 > \lambda_2 > 0$ *with eigengap* $\delta = (\lambda_1 - \lambda_2)/\lambda_1$, *and that* $\langle \tilde{\boldsymbol{u}}_0, \boldsymbol{v}_1 \rangle \geq 1/\sqrt{2}$. *With any* $0 < \epsilon, \xi < 1$, *constant step size*

$\eta > 0$, *and epoch length* T *chosen such that*

$$\eta \leq \frac{c_0 \xi^2}{r^2} \delta, \quad T \geq \frac{c_1 \log(2/\xi)}{\eta \delta}, \quad T \eta^2 r^2 + r \eta \sqrt{T \log(2/\xi)} \leq c_2 \tag{11}$$

for certain universal constants $c_0, c_1, c_2 > 0$, *successive estimates of VR-OPI (summarized in Algorithm 2) after* $S = \lceil \log(1/\epsilon)/\log(2/\xi) \rceil$ *epochs satisfy*

$$|\langle \tilde{\boldsymbol{u}}_S, \boldsymbol{v}_1 \rangle|^2 \geq 1 - \epsilon \tag{12}$$

with probability exceeding $1 - \lceil \log \epsilon \rceil \xi$. *Typical parameter values are* $\eta = 20/m$, $S = 100$, *and* $T = |\bar{\mathcal{I}}_0|$.

The proof of Proposition 1 can be found in [41]. Even though PCA in (7) is nonconvex, the SGD based VR-OPI algorithm converges to the globally optimal solution under mild conditions [41]. Moreover, fixing any $\xi \in (0, 1)$, conditions in (11) hold true when T is chosen to be on the order of $1/(\eta \delta)$, and η to be sufficiently smaller than δ/r^2. Expressed differently, if VR-OPI runs $T = \Theta(r^2/\delta^2)$ iterations per epoch for a total number $S = \Theta(\log(1/\epsilon))$ of epochs, then the returned VR-OPI estimate is ϵ-accurate with probability at least $1 - \lceil \log_2(1/\epsilon) \rceil \xi$. Since each epoch takes $\mathcal{O}(n(T + |\bar{\mathcal{I}}_0|))$ time to implement, the total runtime is of

$$\mathcal{O}\left(n\left(|\bar{\mathcal{I}}_0| + \frac{r^2}{\delta^2}\right) \log(1/\epsilon)\right) \tag{13}$$

which validates the exponential convergence rate of VR-OPI. In addition, when $\delta/r \geq \Omega(1/\sqrt{|\bar{\mathcal{I}}_0|})$, the total runtime reduces to $\mathcal{O}(n|\bar{\mathcal{I}}_0| \log(1/\epsilon))$ up to log-factors. It is worth emphasizing that the required runtime is proportional to the time required to scan the selected data once, which is in stark contrast to the runtime of $\mathcal{O}(n|\bar{\mathcal{I}}_0| \log(1/\epsilon)/\delta)$ when using power method [40]. Simulated tests in Section IV corroborate the effectiveness of VR-OPI over the popular power method in processing data involving large dimensions m and/or n.

C. Stochastic Truncated Gradient Stage

Driven by the need of efficiently processing large-scale phaseless data in imaging applications, a stochastic solution algorithm is put forth for minimizing the amplitude-based cost function in (4). To ensure good performance, the gradient regularization rule in (10) is also accounted for to lead to our truncated stochastic gradient iterations. It is worth mentioning that the Kaczmarz method [44] was also used for solving a system of phaseless quadratic equations in [35]. However, Kaczmarz variants of block or randomized updates converge to at most a neighborhood of the optimal solution $\boldsymbol{x}$. Distance between the Kaczmarz estimates and $\boldsymbol{x}$ is bounded in terms of the dimension m and the size of the amplitude data vector $\boldsymbol{\psi}$ measured by the ℓ_1- or ℓ_∞-norm. Nevertheless, the obtained bounds of the form $m\|\boldsymbol{\psi}\|_1$ or $m\|\boldsymbol{\psi}\|_\infty$ are rather loose (m typically very large), and less attractive than the geometric convergence to the global solution $\boldsymbol{x}$ to be established for also stochastic iterations based STAF.

Adopting the intensity-based Poisson likelihood function (3), an incremental version of TWF was developed in [36], which provably converges to $\boldsymbol{x}$ in linear time. Albeit achieving

6

improved empirical performance and faster convergence over TWF in terms of the number of passes over the entire data to produce an ϵ-accurate solution [18], the number of measurements it requires for exact recovery is still relatively far from the information-theoretic limits. Specifically for the real-valued Gaussian $\boldsymbol{a}_i$ designs, ITWF requires about $m \geq 3.2n$ noiseless measurements to guarantee exact recovery relative to $4.5n$ for TWF [18]. Recall that TAF achieves exact recovery from about $3n$ measurements [19]. Furthermore, gradient iterations can be easily trapped in saddle points when dealing with nonconvex optimization. In contrast, stochastic iterations are able to escape saddle points, and converge globally to at least a local minimum [25]. Hence, besides the appealing computational advantage, stochastic counterparts of TAF may further improve the performance over TAF, as also asserted by the comparison between ITWF and TWF. In the following, we present two STAF variants: Starting with an initial estimate $\boldsymbol{z}_0$ found using VR-OPI in Algorithm 2, the first variant successively updates $\boldsymbol{z}_0$ through amplitude-based stochastic gradient iterations with a constant step size $\mu > 0$ chosen on the order of $1/n$, while the second operates much like the Kaczmarz method, yet both suitably account for the truncation rule in (10).

For simplicity of exposition, let us rewrite the amplitude-based cost function as follows

$$\underset{\boldsymbol{z}\in\mathbb{R}^n}{\text{minimize}} \quad \ell(\boldsymbol{z}) = \sum_{i=1}^m \ell_i(\boldsymbol{z}) := \frac{1}{2}\sum_{i=1}^m \left(\psi_i - |\boldsymbol{a}_i^{\mathcal{T}}\boldsymbol{z}|\right)^2 \quad (14)$$

where the factor $1/2$ is introduced for notational convenience. It is clear that the cost $\ell(\boldsymbol{z})$ or each $\ell_i(\boldsymbol{z})$ in (14) is nonconvex and nonsmooth; hence, the optimization in (14) is computationally intractable in general [45]. Along the lines of nonconvex paradigms including WF [1], TWF [18], and TAF [19], our approach to solving the problem at hand amounts to iteratively refining the initial estimate $\boldsymbol{z}_0$ by means of truncated stochastic gradient iterations. This is in contrast to (T)WF and TAF, which rely on (truncated) gradient-type iterations [1], [18], [19]. STAF processes one datum at a time and evaluates the generalized gradient of one component function $\ell_{i_t}(\boldsymbol{z})$ for some index $i_t \in \{1, 2, \ldots, m\}$ per iteration $t \geq 0$. Specifically, STAF successively updates $\boldsymbol{z}_0$ using the following truncated stochastic gradient iterations for all $t \geq 0$

$$\boldsymbol{z}_{t+1} = \boldsymbol{z}_t - \mu_t \nabla\ell_{i_t}(\boldsymbol{z}_t)\mathbb{1}_{\{|\boldsymbol{a}_{i_t}^{\mathcal{T}}\boldsymbol{z}_t|/|\boldsymbol{a}_{i_t}^{\mathcal{T}}\boldsymbol{x}|\geq 1/(1+\gamma)\}} \quad (15)$$

with

$$\nabla\ell_{i_t}(\boldsymbol{z}_t) = \left(\boldsymbol{a}_{i_t}^{\mathcal{T}}\boldsymbol{z}_t - \psi_{i_t}\frac{\boldsymbol{a}_{i_t}^{\mathcal{T}}\boldsymbol{z}_t}{|\boldsymbol{a}_{i_t}^{\mathcal{T}}\boldsymbol{z}_t|}\right)\boldsymbol{a}_{i_t} \quad (16)$$

where μ_t is either set to be a constant $\mu > 0$ on the order of $1/n$, or taken as the time-varying one as in Kaczmarz's iteration, namely, $\mu_t = 1/\|\boldsymbol{a}_{i_t}\|^2$ [44]. The index i_t is sampled uniformly at random or with given probabilities from $\{1, 2, \ldots, m\}$, or it simply cycles through the entire set $[m]$. In addition, fixing the truncation threshold to $\gamma = 0.7$, the indicator function $\mathbb{1}_{\{|\boldsymbol{a}_{i_t}^{\mathcal{T}}\boldsymbol{z}_t|/|\boldsymbol{a}_{i_t}^{\mathcal{T}}\boldsymbol{x}|\geq 1/(1+\gamma)\}}$ in (15) takes the value 1, if $|\boldsymbol{a}_{i_t}^{\mathcal{T}}\boldsymbol{z}_t|/|\boldsymbol{a}_{i_t}^{\mathcal{T}}\boldsymbol{x}| \geq 1/(1+\gamma)$ holds true; and 0 otherwise. It is worth stressing that this truncation rule provably rejects 'bad' search directions with high probability. Moreover, this

regularization maintains only gradient components of large enough $|\boldsymbol{a}_i^{\mathcal{T}}\boldsymbol{z}^t|$ values, hence saving the objective function (2) from being non-differentiable at $\boldsymbol{z}^t$ and simplifying the theoretical analysis. In the context of large-scale linear regressions or dynamic tracking, similar ideas such as censoring have been pursued [46], [47], [48]. Numerical tests demonstrating the performance improvement using the stochastic truncated iterations will be presented in Section IV.

Algorithm 3 Stochastic truncated amplitude flow (STAF)

1: **Input:** Data $\{(\boldsymbol{a}_i, \psi_i)\}_{i=1}^m$; maximum number of iterations $T = 500m$; by default, step sizes $\mu = 0.8/n$ or $\mu = 1.2/n$ in the real- or complex-valued Gaussian models, truncation thresholds $|\bar{\mathcal{I}}_0| = \lceil\frac{1}{6}m\rceil$, and $\gamma = 0.7$.

2: **Evaluate** $\bar{\mathcal{I}}_0$ to consist of indices associated with the $|\bar{\mathcal{I}}_0|$ largest values among $\{\psi_i/\|\boldsymbol{a}_i\|\}$.

3: **Initialize** $\boldsymbol{z}_0$ as $\sqrt{\frac{1}{m}\sum_{i=1}^m \psi_i^2}\,\tilde{\boldsymbol{z}}_0$, where $\tilde{\boldsymbol{z}}_0$ is obtained via Algorithm 2 with $\bar{\boldsymbol{Y}}_0 := \frac{1}{|\bar{\mathcal{I}}_0|}\sum_{i\in\bar{\mathcal{I}}_0}\frac{\boldsymbol{a}_i\boldsymbol{a}_i^{\mathcal{T}}}{\|\boldsymbol{a}_i\|^2}$.

4: **For** $t = 0$ **to** $T - 1$ **do**

$$\boldsymbol{z}_{t+1} = \boldsymbol{z}_t - \mu\boldsymbol{a}_{i_t}\left(\boldsymbol{a}_{i_t}^{\mathcal{T}}\boldsymbol{z}_t - \psi_{i_t}\frac{\boldsymbol{a}_{i_t}^{\mathcal{T}}\boldsymbol{z}_t}{|\boldsymbol{a}_{i_t}^{\mathcal{T}}\boldsymbol{z}_t|}\right)\mathbb{1}_{\left\{|\boldsymbol{a}_{i_t}^{\mathcal{T}}\boldsymbol{z}_t|\geq\frac{\psi_{i_t}}{1+\gamma}\right\}}$$
(17)

where i_t is sampled uniformly at random from $\{1, 2, \ldots, m\}$, or,

$$\boldsymbol{z}_{t+1} = \boldsymbol{z}_t - \frac{\boldsymbol{a}_{i_t}}{\|\boldsymbol{a}_{i_t}\|^2}\left(\boldsymbol{a}_{i_t}^{\mathcal{T}}\boldsymbol{z}_t - \psi_{i_t}\frac{\boldsymbol{a}_{i_t}^{\mathcal{T}}\boldsymbol{z}_t}{|\boldsymbol{a}_{i_t}^{\mathcal{T}}\boldsymbol{z}_t|}\right)\mathbb{1}_{\left\{|\boldsymbol{a}_{i_t}^{\mathcal{T}}\boldsymbol{z}_t|\geq\frac{\psi_{i_t}}{1+\gamma}\right\}}$$
(18)

where i_t is sampled at random from $\{1, 2, \ldots, m\}$ with probability proportional to $\|\boldsymbol{a}_{i_t}\|^2$.

5: **End for**

6: **Output:** $\boldsymbol{z}_T$.

III. MAIN RESULTS

The proposed STAF scheme is summarized as Algorithm 3, with either constant step size $\mu > 0$ in the truncated stochastic gradient iterations in (17), or with time-varying step size $\mu_t = 1/\|\boldsymbol{a}_{i_t}\|^2$ in the truncated Kaczmarz iterations in (18). Equipped with an initialization obtained using VR-OPI, both STAF variants will be shown to converge at an exponential rate to the globally optimal solution with high probability, as soon as m/n the number of equations and unknowns exceeds some numerical constant.

Assuming m independent data samples $\{(\boldsymbol{a}_i; \psi_i)\}$ drawn from the real-valued Gaussian model, the following establishes theoretical performance of STAF in the absence of noise.

Theorem 1 (Exact recovery). *Consider the noiseless measurements $\psi_i = |\boldsymbol{a}_i^{\mathcal{T}}\boldsymbol{x}|$ with an arbitrary signal $\boldsymbol{x} \in \mathbb{R}^n$, and i.i.d. $\{\boldsymbol{a}_i \sim \mathcal{N}(\boldsymbol{0}, \boldsymbol{I}_n)\}_{i=1}^m$. If μ_t is either set to be a constant $\mu > 0$ as per (17), or it is time-varying $\mu_t = 1/\|\boldsymbol{a}_{i_t}\|^2$ as per (18) with the corresponding index sampling scheme, and also*

$$m \geq c_0 n \quad and \quad \mu \leq \mu_0/n \quad (19)$$

then with probability at least $1 - c_1 m \exp(-c_2 n)$, the stochastic truncated amplitude flow (STAF) estimates (tabulated in Algorithm 3 with default parameters) satisfy

$$\mathbb{E}_{\mathcal{P}_t} \left[\operatorname{dist}^2(\boldsymbol{z}_t, \boldsymbol{x}) \right] \leq \rho \left(1 - \frac{\nu}{n} \right)^t \|\boldsymbol{x}\|^2, \quad t = 0, 1, \ldots \quad (20)$$

for $\rho = 1/10$ and some numerical constant $\nu > 0$, where the expectation is taken over the path sequence $\mathcal{P}_t := \{i_0, i_1, \ldots, i_{t-1}\}$, and $c_0, c_1, c_2, \mu_0 > 0$ are certain universal constants.

The proof of Theorem 1 is deferred to the Appendix. Apparently, the mean-square distance between the iterate and the global solution is reduced by a factor of $(1 - \nu/n)^m$ after one pass through the entire data. Heed that the expectation $\mathbb{E}_{\mathcal{P}_t}[\cdot]$ in (20) is taken over the algorithmic randomness $\mathcal{P}_t$ rather than the data. This is important since in general the data may be modeled as deterministic. Although only performing stochastic iterations in (17) and (18), STAF still enjoys linear convergence rate. This is in sharp contrast to typical SGD methods, where variance reduction techniques controlling the variance of the stochastic gradients are required to achieve linear convergence rate [43], [41], as in Algorithm 2. Moreover, the largest constant step size that STAF can afford is estimated to be $\mu_0 = 0.8469$, giving rise to a convergence factor of $\nu_0 = 0.0696$ in (20). When truncated Kaczmarz iterations are implemented, ν is estimated to be 1.0091 much larger than the one in the constant step size case. Our experience with numerical experiments also confirm that the Kaczmarz-based STAF in (18) converges faster than the constant step-size based one in (17), yet it is slightly more sensitive when additive noise is present in the data.

IV. Simulated Tests

This section presents extensive numerical experiments evaluating the performance of STAF using both synthetic data and real images. STAF was thoroughly compared with existing alternatives including TAF [19], (T)WF [1], [18], and ITWF [36]. For fair comparisons, all the parameters pertinent to implementation of each algorithm were set to their suggested values. The initialization in each scheme was found based on a number of (power/stochastic) iterations equivalent to 100 passes over the entire data, which was subsequently refined by a number of iterations corresponding to $1,000$ passes; unless otherwise stated. All simulated estimates were averaged over 100 independent Monte Carlo trials. Two performance evaluation metrics were used: the relative root mean-square error defined as Relative error $:= \operatorname{dist}(\boldsymbol{z}, \boldsymbol{x})/\|\boldsymbol{x}\|$; and the empirical successful recovery rate among 100 independent runs, in which a success is declared when the returned estimate incurs a relative error less than 10^{-5} [1]. Tests using both noiseless/noisy real-/complex-valued Gaussian models $\psi_i = |\boldsymbol{a}_i^{\mathcal{H}} \boldsymbol{x}| + \eta_i$ were conducted, where the i.i.d. noise obeys $\eta_i \sim \mathcal{N}(0, \sigma^2 \|\boldsymbol{x}\|^2)$. The Matlab implementations of STAF can be downloaded from http://www.tc.umn.edu/~gangwang/STAF.

The first experiment compares VR-OPI in Algorithm 2 with the power method in Algorithm 1 to solve the orthogonality-promoting initialization optimization in (7). The comparison
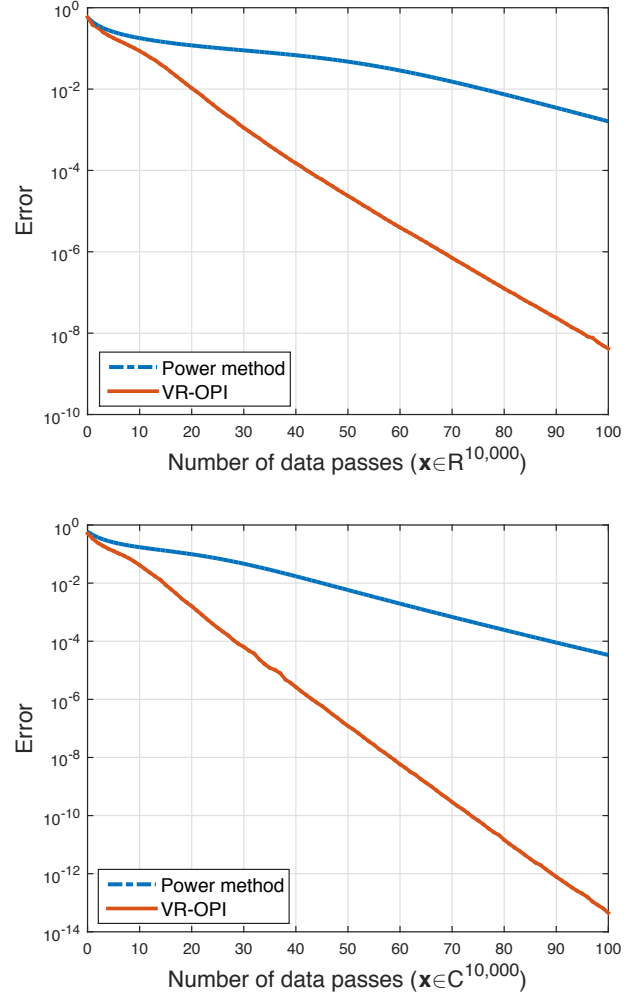

Fig. 2: Error evolution of the iterates using: i) power method in Algorithm 1; and ii) variance-reducing orthogonality-promoting initialization in Algorithm 2 for solving problem (7) with step size $\eta = 1$. Top: Noiseless real-valued Gaussian model with $\boldsymbol{x} \sim \mathcal{N}(\boldsymbol{0}, \boldsymbol{I}_n)$, and $\boldsymbol{a}_i \sim \mathcal{N}(\boldsymbol{0}, \boldsymbol{I}_n)$, where $n = 10^4$, and $m = 2n - 1$. Bottom: Noiseless complex-valued Gaussian model with $\boldsymbol{x} \sim \mathcal{CN}(\boldsymbol{0}, \boldsymbol{I}_n)$, and $\boldsymbol{a}_i \sim \mathcal{CN}(\boldsymbol{0}, \boldsymbol{I}_n)$, where $n = 10^4$, and $m = 4n - 4$.

is carried out in terms of the number of data passes to achieve the same solution accuracy, in which one pass through the selected data amounts to a number $|\overline{\mathcal{I}}_0|$ of gradient evaluations of component functions. First, synthetic data based experiments are conducted using the real-/complex-valued Gaussian models with $n = 10,000$ under the known sufficient conditions for uniqueness, i.e., $m = 2n - 1$ in the real case, and $m = 4n - 4$ in the complex case. Figure 2 plots the error evolution of the iterates $\boldsymbol{u}_t$ for the power method and VR-OPI, where the error in logarithmic scale is defined as $\log_{10}\left(1 - \|\boldsymbol{D}^{\mathcal{T}} \boldsymbol{u}_t\|^2 / \|\boldsymbol{D}^{\mathcal{T}} \boldsymbol{v}_0\|^2\right)$ with the exact principal eigenvector $\boldsymbol{v}_0$ computed from the SVD of $\overline{\boldsymbol{Y}}_0 = \boldsymbol{D} \boldsymbol{D}^{\mathcal{T}}$ in (7). Apparently, the inexpensive stochastic iterations of VR-OPI achieve certain solution accuracy with considerably fewer
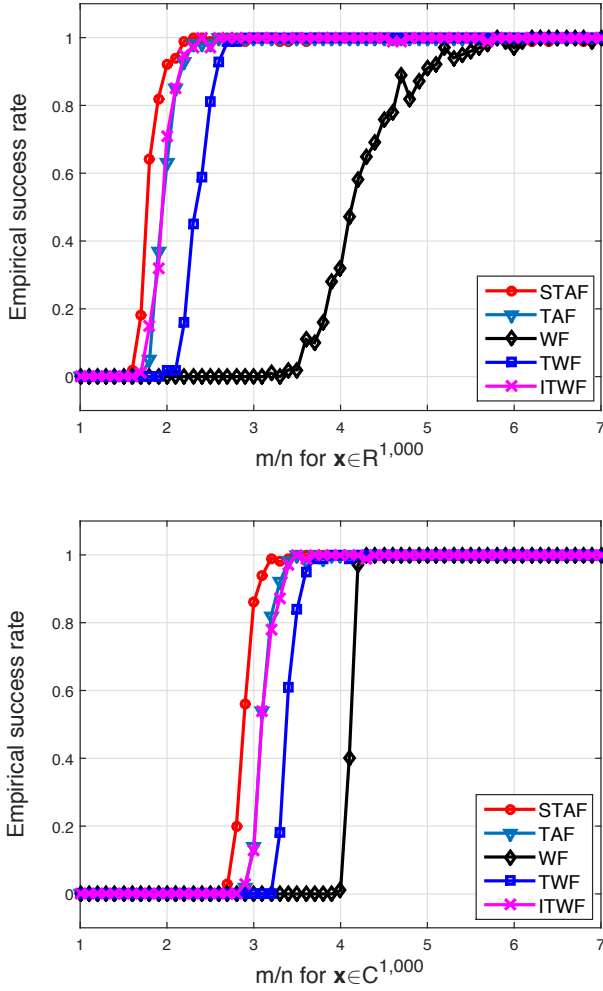
Fig. 3: Empirical success rate for: i) WF [1]; ii) TWF [18]; iii) ITAF [36]; iv) TAF [19]; and v) STAF with $n = 1,000$ and m/n varying by 0.1 from 1 to 7 under the *same* orthogonality-promoting initialization. Top: Noiseless real-valued Gaussian model with $x \sim \mathcal{N}(0, I_n)$, and $a_i \sim \mathcal{N}(0, I_n)$; Bottom: Noiseless complex-valued Gaussian model with $x \sim \mathcal{CN}(0, I_n)$, and $a_i \sim \mathcal{CN}(0, I_n)$.
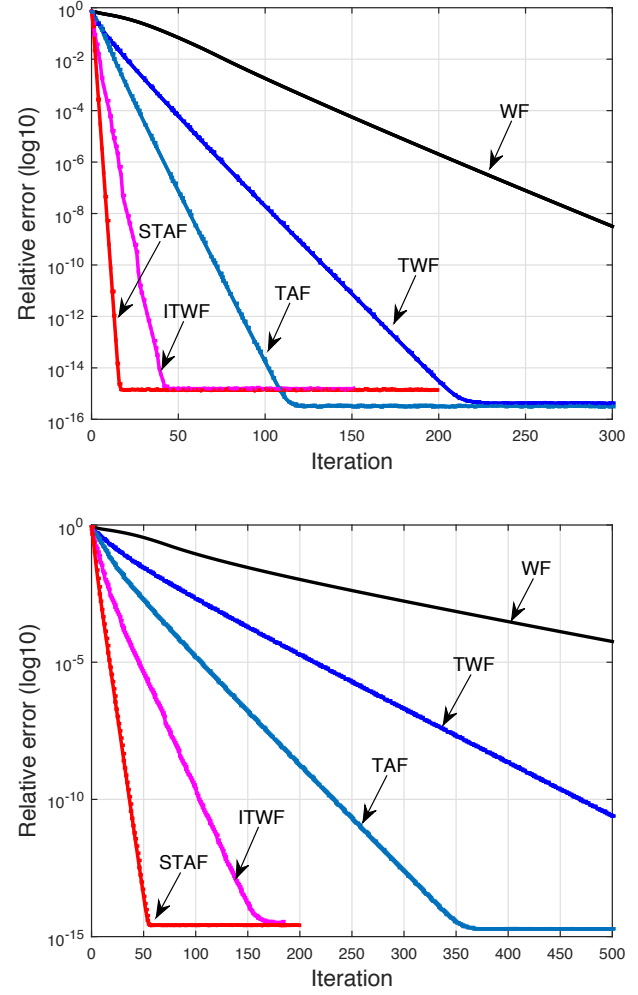
Fig. 4: Relative error versus iterations using: i) WF [1]; ii) TWF [18]; iii) ITAF [36]; iv) TAF [19]; and v) STAF under the *same* orthogonality-promoting initialization. Top: Noiseless real-valued Gaussian model with $x \sim \mathcal{N}(0, I_n)$, and $a_i \sim \mathcal{N}(0, I_n)$; Bottom: Noiseless complex-valued Gaussian model with $x \sim \mathcal{CN}(0, I_n)$, and $a_i \sim \mathcal{CN}(0, I_n)$, where $n = 1,000$, and $m = 5n$.

gradient evaluations or data passes in both real and complex settings. This is important for tasks of large $|\bar{\mathcal{I}}_0|$, or equivalently large dimension m (since $|\bar{\mathcal{I}}_0| = 5m/6$ by default), because one less data pass implies $|\bar{\mathcal{I}}_0|$ fewer gradient evaluations and thus results in considerable savings in computational resources.

The second experiment evaluates the refinement stage of STAF relative to its competing alternatives including those of (T)WF, TAF, and ITWF in a variety of settings. For fairness, all schemes were here initialized using the *same* orthogonality-promoting initialization found using 100 power iterations, and subsequently applied a number of iterations corresponding to $T = 1,000$ data passes. First, tests on the noiseless real- and complex-valued Gaussian models were conducted, with i.i.d. $a_i \sim \mathcal{N}(0, I_{1,000})$, $x \sim \mathcal{N}(0, I_{1,000})$, and i.i.d. $a_i \sim \mathcal{CN}(0, I_{1,000})$, $x \sim \mathcal{CN}(0, I_{1,000})$, respectively. Figure 3 depicts the empirical success rate of all considered

schemes with m/n varying by 0.1 from 1 to 7. Figure 4 compares the convergence speed of various schemes in terms of the number of data passes to produce solutions of a given accuracy. Apparently, starting with the same initialization, STAF outperforms its competing alternatives under both real-/complex-valued Gaussian models. In particular, SGD-based STAF improves in terms of exact recovery and convergence speed over the state-of-the-art gradient-type TAF, corroborating the benefit of using SGD-type solvers to cope with saddle points and local minima of nonconvex optimization [25], [36].

The previous experiment showed improved performance of STAF under the same initialization. Now, we present numerical results comparing different schemes equipped with their own initialization, namely, WF with spectral initialization [1], (I)TWF with truncated spectral initialization [18], as well as TAF with orthogonality-promoting initialization using power
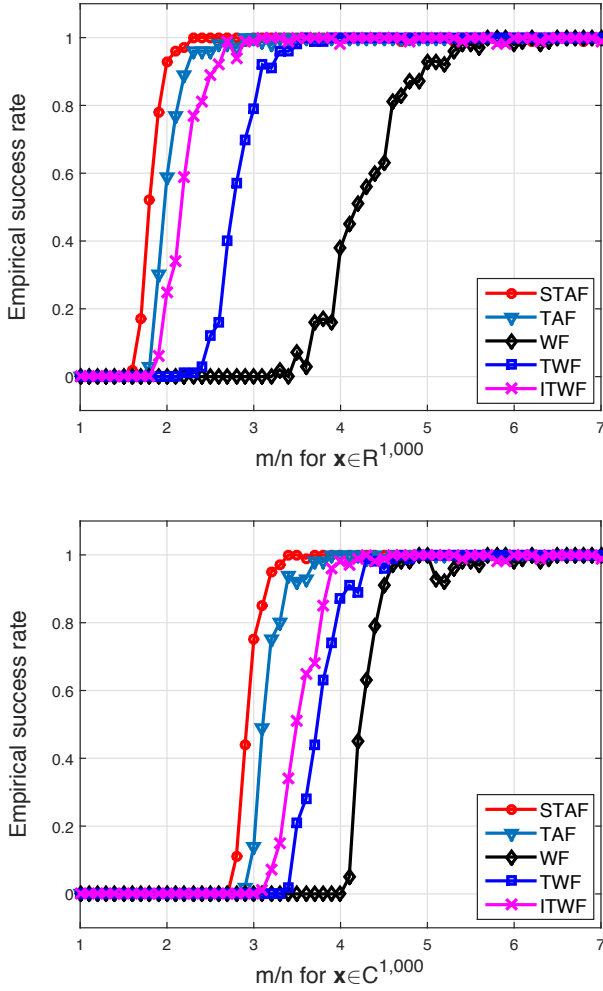
Fig. 5: Empirical success rate for: i) WF [1]; ii) TWF [18]; iii) ITAF [36]; iv) TAF [19]; and v) STAF with $n = 1,000$ and m/n varying 0.1 from 1 to 7. Top: Noiseless real-valued Gaussian model with $\boldsymbol{x} \sim \mathcal{N}(\mathbf{0}, \boldsymbol{I}_n)$, and $\boldsymbol{a}_i \sim \mathcal{N}(\mathbf{0}, \boldsymbol{I}_n)$; Bottom: Noiseless complex-valued Gaussian model with $\boldsymbol{x} \sim \mathcal{CN}(\mathbf{0}, \boldsymbol{I}_n)$, and $\boldsymbol{a}_i \sim \mathcal{CN}(\mathbf{0}, \boldsymbol{I}_n)$.

Fig. 6: Relative error versus iterations using: i) WF [1]; ii) TWF [18]; iii) ITAF [36]; iv) TAF [19]; and v) STAF with $n = 1,000$ and $m/n = 5$. Top: Noisy real-valued Gaussian model with $\boldsymbol{x} \sim \mathcal{N}(\mathbf{0}, \boldsymbol{I}_n)$, and $\boldsymbol{a}_i \sim \mathcal{N}(\mathbf{0}, \boldsymbol{I}_n)$; Bottom: Noisy complex-valued Gaussian model with $\boldsymbol{x} \sim \mathcal{CN}(\mathbf{0}, \boldsymbol{I}_n)$, and $\boldsymbol{a}_i \sim \mathcal{CN}(\mathbf{0}, \boldsymbol{I}_n)$.

iterations [19], and STAF with VR-OPI. Figure 5 demonstrates merits of STAF over its competing alternatives in exact recovery performance on the noiseless real-valued (left) and complex-valued (right) Gaussian model. Specifically in the real case, STAF guarantees exact recovery from about $2.3n$ magnitude-only measurements, which is close to the information-theoretic limit of $m = 2n-1$. In comparison, existing alternatives require a few times more measurements to achieve exact recovery. STAF also performs well in the complex case.

To demonstrate the robustness of STAF against additive noise, we perform stable phase retrieval under the noisy real-/complex-valued Gaussian model $\psi_i = |\boldsymbol{a}_i^{\mathcal{H}}\boldsymbol{x}| + \eta_i$, with $\eta_i \sim \mathcal{N}(0, \sigma^2\boldsymbol{I})$ i.i.d., and $\sigma^2 = 0.1^2\|\boldsymbol{x}\|^2$. The noisy data for magnitude-square based algorithms were generated as $y_i = \psi_i^2$. Curves in Fig. 6 clearly show near-perfect statistical performance and fast convergence of STAF.

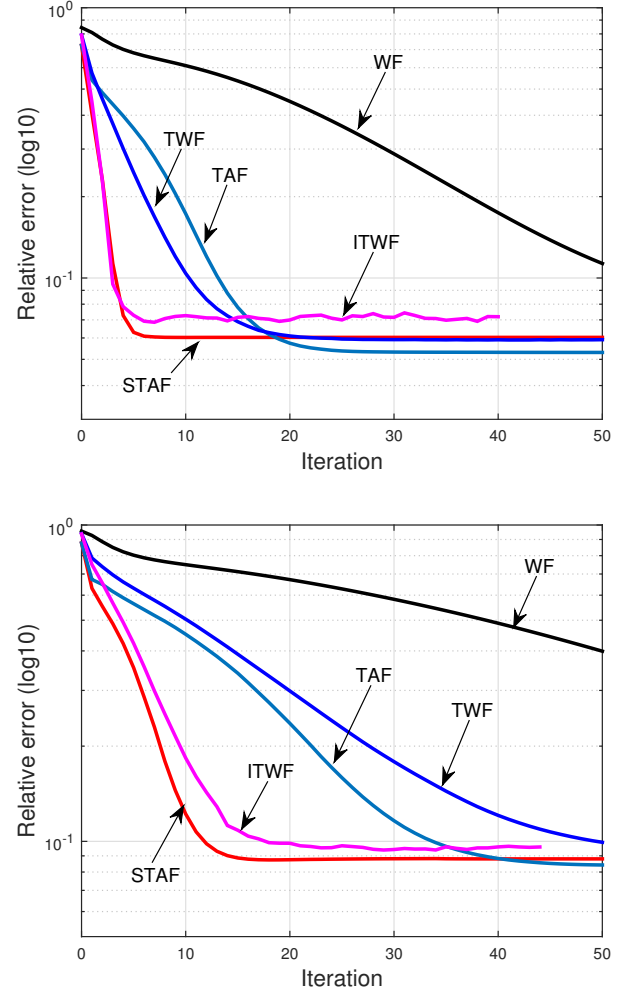Finally, to demonstrate the effectiveness and scalability

of STAF on real data, the Milky Way Galaxy image[1] is considered. The colorful image of RGB bands is denoted by $\boldsymbol{X} \in \mathbb{R}^{1080 \times 1920 \times 3}$, in which the first two indices encode the pixel location, and the third the color band. The algorithm was run independently on each of the three RGB images. We collected the physically realizable measurements called coded diffraction patterns (CDP) using random masks [17], which have also been used in [1], [18], [19], [36]. Letting $\boldsymbol{x} \in \mathbb{R}^n$ be a vectorization of a certain band of $\boldsymbol{X}$, one has magnitude measurements of the form

$$\boldsymbol{\psi}^{(k)} = \left| \boldsymbol{F} \boldsymbol{D}^{(k)} \boldsymbol{x} \right|, \quad 1 \leq k \leq K \qquad (21)$$

where $n = 1,080 \times 1,920 = 2,073,600$, $\boldsymbol{F}$ is an $n \times n$ discrete Fourier transform matrix, and $\boldsymbol{D}^{(k)}$ is a diagonal matrix whose diagonal entries are sampled uniformly at random from phase

---

[1]Downloaded from http://pics-about-space.com/milky-way-galaxy.

delays $\{1, -1, j, -j\}$, with j denoting the imaginary unit. CDP measurements were generated using $K = 8$ random masks for a total of $m = nK$ measurements. In this part, since the fast Fourier transform (FFT) can be implemented in $\mathcal{O}(n \log n)$ instead of $\mathcal{O}(n^2)$ operations, the advantage of using STAF with optimal per-iteration complexity is less pronounced. Hence, instead of processing one quadratic measurement per iteration, a block STAF version processes per iteration n^2 measurements associated with one random mask. That is, STAF samples randomly the index $k \in \{1, 2, \ldots, K\}$ of masks in (21), and updates the iterate using all diffraction patterns corresponding to the k-th mask. In this case, STAF is able to leverage the efficient implementation of FFT, and converges fast. Figure 7 displays the recovered images, where the top is obtained after 100 data passes of VR-OPI iterations, and the bottom is produced by 100 data passes of STAF iterations refining the initialization. Apparently, the recovered images corroborate the effectiveness of STAF in real-world conditions.

V. CONCLUDING REMARKS

This paper developed a new linear-time algorithm abbreviated with STAF to solve systems of quadratic equations, and considerably broaden the scope of the state-of-the-art TAF algorithm in [19]. Adopting the amplitude-based nonconvex formulation, STAF is a two-stage iterative algorithm. It first adopts an orthogonality-promoting initialization using a stochastic variance reduced gradient algorithm, and subsequently refines the initial estimate via truncated stochastic amplitude-based iterations. STAF was shown capable of recovering any signal from about as many equations as unknowns. In contrast to existing alternatives, both stages of STAF achieve optimal iteration and computational complexities that make it attractive to large-scale implementation. Numerical tests involving synthetic data and real images corroborate the merits of STAF in terms of both exact recovery performance and convergence speed over the state-of-the-art approaches including TAF, (T)WF, and ITWF.

Pertinent future research directions include establishing analytical results for STAF in the presence of noise, and comparing the estimation performance of STAF with known Cramer-Rao bounds [29]. Another possibility consists of leveraging the orthogonality-promoting initialization in the context of robust phase retrieval and faster semidefinite optimization, and developing suitable gradient regularization rules for other nonconvex optimization tasks. Devising inexpensive stochastic iterations based solvers for compressive phase retrieval, as well as generalization to two-dimensional phase retrieval problems, constitute additional research directions for future research.

APPENDIX

PROOF FOR THEOREM 1

Recall from [19, Thm.1] that when m/n exceeds some universal constant $c_0 > 0$, the estimate $\boldsymbol{z}_0$ returned by the orthogonality-promoting initialization obeys the following with high probability

$$\text{dist}(\boldsymbol{z}_0, \boldsymbol{x}) \leq (1/10)\|\boldsymbol{x}\|. \tag{22}$$

Along the lines of (T)WF and TAF, to prove our Theorem 1, it suffices to show that successive STAF iterates $\boldsymbol{z}_t$ are on average locally contractive around the planted solution $\boldsymbol{x}$, as asserted in the following proposition. See the Appendix for proof details.

Proposition 2 (Local error contraction). *Consider the noise-less measurements $\psi_i = |\boldsymbol{a}_i^T \boldsymbol{x}|$ with an arbitrary signal $\boldsymbol{x} \in \mathbb{R}^n$, and i.i.d. $\boldsymbol{a}_i \sim \mathcal{N}(\boldsymbol{0}, \boldsymbol{I}_n)$, $1 \leq i \leq m$. Under the default algorithmic parameters given in Algorithm 3, there exist universal constants $c_0', c_1', c_2' > 0$, and $\nu > 0$, such that with probability at least $1 - c_2' m \exp(-c_1' n)$, the following holds simultaneously for all $\boldsymbol{z}_t$ satisfying (22)*

$$\mathbb{E}_{i_t} \left[\text{dist}^2(\boldsymbol{z}_{t+1}, \boldsymbol{x}) \right] \leq \left(1 - \frac{\nu}{n} \right) \text{dist}^2(\boldsymbol{z}_t, \boldsymbol{x}) \tag{23}$$

provided that $m \geq c_0' n$.

Proposition 2 demonstrates monotonic decrease of the mean-square estimation error: Once entering a reasonably small-size neighborhood of $\boldsymbol{x}$, successive iterates of STAF will be dragged toward $\boldsymbol{x}$ at a linear rate. Upon establishing the local error contraction property in (23), taking expectation on both sides of (23) over i_{t-1}, and applying Proposition 2 again, yields a similar relation for the previous iteration. Continuing this process to reach the initialization $\boldsymbol{z}_0$ and appealing to the initialization result in (22) collectively, leads to (20), hence completes the proof of Thm. 1.

PROOF OF PROPOSITION 2

To prove Proposition 2, let us first define the truncated gradient of $\ell(\boldsymbol{z})$ as follows

$$\nabla \ell_{\text{tr}}(\boldsymbol{z}) = \sum_{i=1}^{m} \left(\boldsymbol{a}_i^T \boldsymbol{z} - \psi_i \frac{\boldsymbol{a}_i^T \boldsymbol{z}}{|\boldsymbol{a}_i^T \boldsymbol{z}|} \right) \boldsymbol{a}_i \mathbb{1}_{\left\{ |\boldsymbol{a}_i^T \boldsymbol{z}_t| \geq \frac{1}{1+\gamma} \psi_i \right\}} \tag{24}$$

which corresponds to the truncated gradient employed by TAF [19]. Instrumental in proving the local error contraction in Proposition 2, the following lemma adopts a sufficient decrease result from [19, Proposition 3]. The sufficient decrease is a key step in establishing the local regularity condition [1], [18], [19], which suffices to prove linear convergence of iterative optimization algorithms.

Proposition 3. *[19, Proposition 3] Consider the noise-free measurements $\psi_i = |\boldsymbol{a}_i^T \boldsymbol{x}|$ with i.i.d. $\boldsymbol{a}_i \sim \mathcal{N}(\boldsymbol{0}, \boldsymbol{I}_n)$, $1 \leq i \leq m$, and $\gamma = 0.7$. For any fixed $\epsilon > 0$, there exist universal constants $c_0', c_1', c_2' > 0$ such that if $m > c_0' n$, then the following holds with probability at least $1 - c_2' \exp(-c_1' m)$,*

$$\left\langle \boldsymbol{h}, \frac{1}{m} \nabla \ell_{\text{tr}}(\boldsymbol{z}) \right\rangle \geq 2 \left(1 - \zeta_1 - \zeta_2 - 2\epsilon \right) \|\boldsymbol{h}\|^2, \quad \boldsymbol{h} := \boldsymbol{z} - \boldsymbol{x} \tag{25}$$

for all $\boldsymbol{x}, \boldsymbol{z} \in \mathbb{R}^n$ such that $\|\boldsymbol{h}\|/\|\boldsymbol{x}\| \leq 1/10$, where estimates $\zeta_1 \approx 0.0782$, and $\zeta_2 \approx 0.3894$.
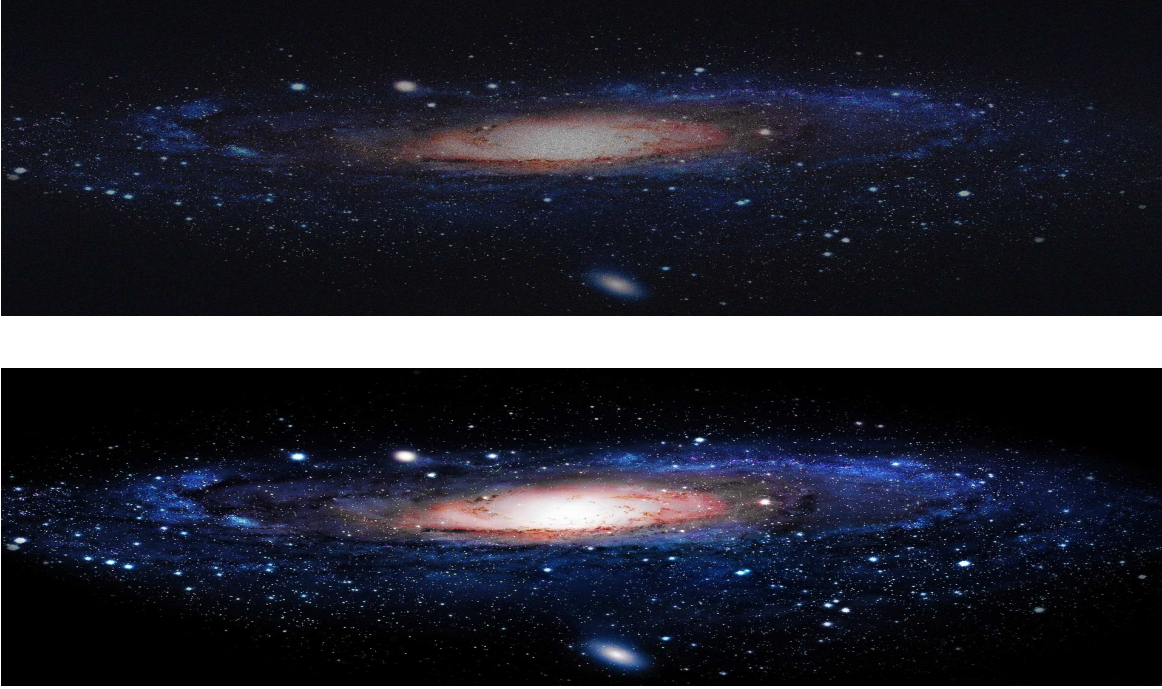
Fig. 7: Recovered images after: the variance-reducing orthogonality-promoting initialization stage (top panel), and the STAF refinement stage (bottom panel) on the Milky Way Galaxy image using $K = 8$ random masks.

Now let us turn to the term on the left hand side of (23), which after plugging in the update of z_{t+1} in (17) or (18), boils down to

$$
\begin{aligned}
&\mathrm{dist}^2(z_{t+1}, x) \\
&= \left\| h_t - \mu_t \left(a_{i_t}^{\mathcal{T}} z_t - \psi_{i_t} \frac{a_{i_t}^{\mathcal{T}} z_t}{|a_{i_t}^{\mathcal{T}} z_t|} \right) a_{i_t} \mathbb{1}_{\left\{ |a_{i_t}^{\mathcal{T}} z_t| \geq \frac{\psi_{i_t}}{1+\gamma} \right\}} \right\|^2 \\
&= \|h_t\|^2 - 2\mu_t \left(a_{i_t}^{\mathcal{T}} z_t - \psi_{i_t} \frac{a_{i_t}^{\mathcal{T}} z_t}{|a_{i_t}^{\mathcal{T}} z_t|} \right) a_{i_t}^{\mathcal{T}} h_t \mathbb{1}_{\left\{ |a_{i_t}^{\mathcal{T}} z_t| \geq \frac{\psi_{i_t}}{1+\gamma} \right\}} \\
&\quad + \mu_t^2 \left(a_{i_t}^{\mathcal{T}} z_t - \psi_{i_t} \frac{a_{i_t}^{\mathcal{T}} z_t}{|a_{i_t}^{\mathcal{T}} z_t|} \right)^2 \|a_{i_t}\|^2 \mathbb{1}_{\left\{ |a_{i_t}^{\mathcal{T}} z_t| \geq \frac{\psi_{i_t}}{1+\gamma} \right\}} \quad (26)
\end{aligned}
$$

where $\mu_t = \mu > 0$ with $i_t \in \{1, 2, \ldots, m\}$ sampled uniformly at random in (17), or $\mu_t = 1/\|a_{i_t}\|^2$ with $i_t \in \{1, 2, \ldots, m\}$ selected with probability proportional to $\|a_{i_t}\|^2$ in (18).

Consider first the constant step size case in (17). Take the expectation of both sides in (26) with respect to the selection of index i_t (rather than the data randomness) to obtain

$$
\begin{aligned}
&\mathbb{E}_{i_t}\left[\mathrm{dist}^2(z_{t+1}, x) \right] \\
&= \|h_t\|^2 - \frac{2\mu}{m} \sum_{i_t=1}^m \left(a_{i_t}^{\mathcal{T}} z_t - \psi_{i_t} \frac{a_{i_t}^{\mathcal{T}} z_t}{|a_{i_t}^{\mathcal{T}} z_t|} \right) a_{i_t}^{\mathcal{T}} h_t \mathbb{1}_{\left\{ |a_{i_t}^{\mathcal{T}} z_t| \geq \frac{\psi_{i_t}}{1+\gamma} \right\}} \\
&\quad + \frac{\mu^2}{m} \sum_{i_t=1}^m \left(a_{i_t}^{\mathcal{T}} z_t - \psi_{i_t} \frac{a_{i_t}^{\mathcal{T}} z_t}{|a_{i_t}^{\mathcal{T}} z_t|} \right)^2 \|a_{i_t}\|^2 \mathbb{1}_{\left\{ |a_{i_t}^{\mathcal{T}} z_t| \geq \frac{\psi_{i_t}}{1+\gamma} \right\}}.
\end{aligned}
$$
$$(27)$$

Now the task reduces to upper bounding the terms on the right hand side of (27). Note from (24) that by means of $\nabla \ell_{\mathrm{tr}}(z_t)$,

the second term in (27) can be re-expressed as follows

$$
\begin{aligned}
&-\frac{2\mu}{m} \sum_{i_t=1}^m \left(a_{i_t}^{\mathcal{T}} z_t - \psi_{i_t} \frac{a_{i_t}^{\mathcal{T}} z_t}{|a_{i_t}^{\mathcal{T}} z_t|} \right) a_{i_t}^{\mathcal{T}} h_t \mathbb{1}_{\left\{ |a_{i_t}^{\mathcal{T}} z_t| \geq \frac{\psi_{i_t}}{1+\gamma} \right\}} \\
&= -\frac{2\mu}{m} \langle \nabla \ell_{\mathrm{tr}}(z_t), h_t \rangle \\
&\leq -4\mu \left(1 - \zeta_1 - \zeta_2 - 2\epsilon \right) \|h\|^2 \quad (28)
\end{aligned}
$$

where the inequality follows from Proposition 3. Regarding the last term in (27), since for the i.i.d. real-valued Gaussian a_i's, $\max_{i_t \in [m]} \|a_{i_t}\| \leq 2.3n$ holds with probability at least $1 - me^{-n/2}$ [19], and also $\mathbb{1}_{\left\{ |a_{i_t}^{\mathcal{T}} z_t| \geq \frac{\psi_{i_t}}{1+\gamma} \right\}} \leq 1$, then the next holds with high probability

$$
\begin{aligned}
&\frac{\mu^2}{m} \sum_{i_t=1}^m \left(a_{i_t}^{\mathcal{T}} z_t - \psi_{i_t} \frac{a_{i_t}^{\mathcal{T}} z_t}{|a_{i_t}^{\mathcal{T}} z_t|} \right)^2 \|a_{i_t}\|^2 \mathbb{1}_{\left\{ |a_{i_t}^{\mathcal{T}} z_t| \geq \frac{\psi_{i_t}}{1+\gamma} \right\}} \\
&\leq \frac{2.3n\mu^2}{m} \sum_{i_t=1}^m \left(|a_{i_t}^{\mathcal{T}} z_t| - |a_{i_t}^{\mathcal{T}} x| \right)^2 \\
&\leq \frac{2.3n\mu^2}{m} \sum_{i_t=1}^m \left(a_{i_t}^{\mathcal{T}} z_t - a_{i_t}^{\mathcal{T}} x \right)^2 \\
&\leq \frac{2.3n\mu^2}{m} h_t^{\mathcal{T}} A^{\mathcal{T}} A h_t \\
&\leq 2.3(1+\delta)\mu^2 n \|h_t\|^2 \quad (29)
\end{aligned}
$$

in which the second inequality comes from $(|a_{i_t}^{\mathcal{T}} z_t| - |a_{i_t}^{\mathcal{T}} x|)^2 \leq (a_{i_t}^{\mathcal{T}} z_t - a_{i_t}^{\mathcal{T}} x)^2$, and the last inequality arises due to the fact that $\lambda_{\max}(A^{\mathcal{T}} A) \leq (1+\delta)m$ holds with probability at least $1 - c_2' \exp(-c_1' n\delta^2)$, provided that $m \geq c_0' n\delta^{-2}$ for some universal constant c_0', c_1', $c_2' > 0$ [49, Theorem 5.39].

Substituting (28) and (29) into (27) establishes that

$$\mathbb{E}_{i_t}\left[\mathrm{dist}^2(\boldsymbol{z}_{t+1}, \boldsymbol{x})\right] \leq \left[1 - 4\mu\left(1 - \zeta_1 - \zeta_2 - 2\epsilon\right)\right.$$
$$\left. + 2.3(1+\delta)\mu^2 n\right]\|\boldsymbol{h}_t\|^2 \qquad (30)$$

holds with probability exceeding $1 - c_2 m \exp(-c_1 n)$ provided that $m \geq c_0 n$, where $c_0 \geq c_0' \delta^{-2}$. To obtain legitimate estimates for the step size, fixing $\epsilon, \delta > 0$ to be sufficiently small constants, say e.g., 0.01, then using (30), μ can be chosen such that $4(0.98 - \zeta_1 - \zeta_2) - 2.42\mu n > 0$, yielding

$$0 < \mu < \frac{4(0.98 - \zeta_1 - \zeta_2)}{2.42n} \approx \frac{0.8469}{n} := \frac{\mu_0}{n}. \qquad (31)$$

Plugging $\mu = c_3/n$ for some $0 < c_3 \leq \mu_0$ into (30), gives rise to

$$\mathbb{E}_{i_t}\left[\mathrm{dist}^2(\boldsymbol{z}_{t+1}, \boldsymbol{x})\right] \leq \left(1 - \frac{\nu}{n}\right)\mathrm{dist}^2(\boldsymbol{z}_t, \boldsymbol{x}) \qquad (32)$$

for $\nu := 4c_3(1 - \zeta_1 - \zeta_2 - 2\epsilon) - 2.3c_3^2(1+\delta) \leq \nu_0 := 0.0697$, where the equality holds at the maximum step size $\mu = \mu_0$, hence concluding the proof of Proposition 2 for the constant step size case.

Now let us turn to the case of a time-varying step size. Specifically, let $\mu_t = 1/\|\boldsymbol{a}_{i_t}\|^2$, and i_t be sampled at random from the set $\{1, 2, \ldots, m\}$ with probability $\|\boldsymbol{a}_{i_t}\|^2 / \sum_{i_t=1}^m \|\boldsymbol{a}_{i_t}\|^2 = \|\boldsymbol{a}_{i_t}\|^2 / \|\boldsymbol{A}\|_F^2$ [50]. Taking the expectation of both sides in (26) over i_t gives rise to

$$\mathbb{E}_{i_t}\left[\mathrm{dist}^2(\boldsymbol{z}_{t+1}, \boldsymbol{x})\right]$$
$$= \|\boldsymbol{h}_t\|^2 - 2\sum_{i_t=1}^m \frac{\boldsymbol{a}_{i_t}^\mathcal{T}\boldsymbol{h}_t}{\|\boldsymbol{A}\|_F^2}\left(\boldsymbol{a}_{i_t}^\mathcal{T}\boldsymbol{z}_t - \psi_{i_t}\frac{\boldsymbol{a}_{i_t}^\mathcal{T}\boldsymbol{z}_t}{|\boldsymbol{a}_{i_t}^\mathcal{T}\boldsymbol{z}_t|}\right)\mathbb{1}_{\left\{|\boldsymbol{a}_{i_t}^\mathcal{T}\boldsymbol{z}_t|\geq\frac{\psi_{i_t}}{1+\gamma}\right\}}$$
$$+ \sum_{i_t=1}^m \frac{1}{\|\boldsymbol{A}\|_F^2}\left(\boldsymbol{a}_{i_t}^\mathcal{T}\boldsymbol{z}_t - \psi_{i_t}\frac{\boldsymbol{a}_{i_t}^\mathcal{T}\boldsymbol{z}_t}{|\boldsymbol{a}_{i_t}^\mathcal{T}\boldsymbol{z}_t|}\right)^2\mathbb{1}_{\left\{|\boldsymbol{a}_{i_t}^\mathcal{T}\boldsymbol{z}_t|\geq\frac{\psi_{i_t}}{1+\gamma}\right\}}. \qquad (33)$$

Consider random $\boldsymbol{A} := [\boldsymbol{a}_1 \cdots \boldsymbol{a}_m]^\mathcal{T}$ with i.i.d. rows $\boldsymbol{a}_i \sim \mathcal{N}(\boldsymbol{0}, \boldsymbol{I}_n)$, and any fixed $\sigma > 0$. Then, by means of Bernstein-type inequality [49, Proposition 5.16], $\left|\frac{1}{mn}\|\boldsymbol{A}\|_F^2 - 1\right| = \left|\frac{1}{mn}\sum_{i,j}a_{i,j}^2 - 1\right| \leq \sigma$ holds with probability at least $1 - 2\exp(-mn\sigma^2/8)$. Therefore, the second term on the right hand side of (33) can be bounded as follows

$$-\frac{2}{\|\boldsymbol{A}\|_F^2}\sum_{i_t=1}^m\left(\boldsymbol{a}_{i_t}^\mathcal{T}\boldsymbol{z}_t - \psi_{i_t}\frac{\boldsymbol{a}_{i_t}^\mathcal{T}\boldsymbol{z}_t}{|\boldsymbol{a}_{i_t}^\mathcal{T}\boldsymbol{z}_t|}\right)\boldsymbol{a}_{i_t}^\mathcal{T}\boldsymbol{h}_t\mathbb{1}_{\left\{|\boldsymbol{a}_{i_t}^\mathcal{T}\boldsymbol{z}_t|\geq\frac{\psi_{i_t}}{1+\gamma}\right\}}$$
$$\leq -\frac{2}{(1+\sigma)mn}\sum_{i_t=1}^m\left(\boldsymbol{a}_{i_t}^\mathcal{T}\boldsymbol{z}_t - \psi_{i_t}\frac{\boldsymbol{a}_{i_t}^\mathcal{T}\boldsymbol{z}_t}{|\boldsymbol{a}_{i_t}^\mathcal{T}\boldsymbol{z}_t|}\right)\boldsymbol{a}_{i_t}^\mathcal{T}\boldsymbol{h}_t\mathbb{1}_{\left\{|\boldsymbol{a}_{i_t}^\mathcal{T}\boldsymbol{z}_t|\geq\frac{\psi_{i_t}}{1+\gamma}\right\}}$$
$$\leq -\frac{4m}{(1+\sigma)mn}(1 - \zeta_1 - \zeta_2 - 2\epsilon)\|\boldsymbol{h}\|^2$$
$$\leq -\frac{4}{(1+\sigma)n}(1 - \zeta_1 - \zeta_2 - 2\epsilon)\|\boldsymbol{h}\|^2 \qquad (34)$$

where the second inequality follows from Proposition 3, and the last inequality from the fact that $m \geq c_0 n$. Concerning the

last term on the right hand side of (33), one obtains that

$$\sum_{i_t=1}^m \frac{\|\boldsymbol{a}_{i_t}\|^2}{\|\boldsymbol{A}\|_F^2}\frac{1}{\|\boldsymbol{a}_{i_t}\|^2}\left(\boldsymbol{a}_{i_t}^\mathcal{T}\boldsymbol{z}_t - \psi_{i_t}\frac{\boldsymbol{a}_{i_t}^\mathcal{T}\boldsymbol{z}_t}{|\boldsymbol{a}_{i_t}^\mathcal{T}\boldsymbol{z}_t|}\right)^2\mathbb{1}_{\left\{|\boldsymbol{a}_{i_t}^\mathcal{T}\boldsymbol{z}_t|\geq\frac{\psi_{i_t}}{1+\gamma}\right\}}$$
$$= \frac{1}{\|\boldsymbol{A}\|_F^2}\sum_{i_t=1}^m\left(|\boldsymbol{a}_{i_t}^\mathcal{T}\boldsymbol{z}_t| - |\boldsymbol{a}_{i_t}^\mathcal{T}\boldsymbol{x}|\right)^2\mathbb{1}_{\left\{|\boldsymbol{a}_{i_t}^\mathcal{T}\boldsymbol{z}_t|\geq\frac{\psi_{i_t}}{1+\gamma}\right\}}$$
$$\leq \frac{1}{\|\boldsymbol{A}\|_F^2}\sum_{i_t=1}^m\left(\boldsymbol{a}_{i_t}^\mathcal{T}\boldsymbol{z}_t - \boldsymbol{a}_{i_t}^\mathcal{T}\boldsymbol{x}\right)^2$$
$$\leq \frac{1}{\|\boldsymbol{A}\|_F^2}\boldsymbol{h}_t^\mathcal{T}\boldsymbol{A}^\mathcal{T}\boldsymbol{A}\boldsymbol{h}_t$$
$$\leq \frac{(1+\delta)m}{(1-\sigma)mn}\|\boldsymbol{h}_t\|^2$$
$$\leq \frac{(1+\delta)}{(1-\sigma)n}\|\boldsymbol{h}_t\|^2 \qquad (35)$$

which holds with high probability as soon as $m \geq c_0 n \geq c_0' \delta^{-2} n$.

Putting results in (33), (34), and (35) together, one establishes that the following holds

$$\mathbb{E}_{i_t}\left[\mathrm{dist}^2(\boldsymbol{z}_{t+1}, \boldsymbol{x})\right] \leq \left[1 - \frac{4}{(1+\sigma)n}(1 - \zeta_1 - \zeta_2 - 2\epsilon)\right.$$
$$\left. + \frac{(1+\delta)}{(1-\sigma)n}\right]\|\boldsymbol{h}_t\|^2 \qquad (36)$$

with probability at least $1 - c_2 m \exp(-c_1 n)$ provided that $m \geq c_0 n$. Hence, one can set in this case

$$\nu := \frac{4}{(1+\sigma)n}(1 - \zeta_1 - \zeta_2 - 2\epsilon) - \frac{(1+\delta)}{(1-\sigma)n}.$$

Taking without loss of generality δ, σ, ϵ to be 0.01, and substituting the estimates of ζ_1, ζ_2 into (36), one arrives at $\nu = 1.0091$ to deduce that

$$\mathbb{E}_{i_t}\left[\mathrm{dist}^2(\boldsymbol{z}_{t+1}, \boldsymbol{x})\right] \leq \left(1 - \frac{1.0091}{n}\right)\mathrm{dist}^2(\boldsymbol{z}_t, \boldsymbol{x}) \qquad (37)$$

which holds with high probability as soon as $m \geq c_0 n$, establishing the local error contraction property of the truncated Kaczmarz iterations in (18), as claimed in Proposition 2.

Combining the results in (32) and (37), we proved the local error contraction property in Proposition 2 of the two STAF variants under both constant and time-varying step sizes.

REFERENCES

[1] E. J. Candès, X. Li, and M. Soltanolkotabi, "Phase retrieval via Wirtinger flow: Theory and algorithms," *IEEE Trans. Inf. Theory*, vol. 61, no. 4, pp. 1985–2007, Apr. 2015.

[2] J. Miao, P. Charalambous, J. Kirz, and D. Sayre, "Extending the methodology of X-ray crystallography to allow imaging of micrometre-sized non-crystalline specimens," *Nature*, vol. 400, no. 6742, pp. 342–344, July 1999.

[3] R. P. Millane, "Phase retrieval in crystallography and optics," *J. Opt. Soc. Am. A*, vol. 7, no. 3, pp. 394–411, 1990.

[4] O. Bunk, A. Diaz, F. Pfeiffer, C. David, B. Schmitt, D. K. Satapathy, and J. F. van der Veen, "Diffractive imaging for periodic samples: Retrieving one-dimensional concentration profiles across microfluidic channels," *Acta. Crystallogr. A. Found. Crystallogr.*, vol. 63, no. 4, pp. 306–314, 2007.

[5] K. Jaganathan, Y. C. Eldar, and B. Hassibi, "Phase retrieval: An overview of recent developments," *arXiv:1510.07713*, 2015.

This article has been accepted for publication in a future issue of this journal, but has not been fully edited. Content may change prior to final publication. Citation information: DOI 10.1109/TSP.2017.2652392, IEEE Transactions on Signal Processing

13

[6] E. J. Candès, Y. C. Eldar, T. Strohmer, and V. Voroninski, "Phase retrieval via matrix completion," *SIAM Rev.*, vol. 57, no. 2, pp. 225–251, May 2015.

[7] E. Hofstetter, "Construction of time-limited functions with specified autocorrelation functions," *IEEE Trans. Inf. Theory*, vol. 10, no. 2, pp. 119–126, Apr. 1964.

[8] Y. Shechtman, A. Beck, and Y. C. Eldar, "GESPAR: Efficient phase retrieval of sparse signals," *IEEE Trans. Signal Process.*, vol. 62, no. 4, pp. 928–938, Feb. 2014.

[9] J. R. Fienup, "Phase retrieval algorithms: A comparison," *Appl. Opt.*, vol. 21, no. 15, pp. 2758–2769, Aug. 1982.

[10] J. Ranieri, A. Chebira, Y. M. Lu, and M. Vetterli, "Phase retrieval for sparse signals: Uniqueness conditions," *arXiv:1308.3058*, 2013.

[11] K. Jaganathan, S. Oymak, and B. Hassibi, "Recovery of sparse 1-D signals from the magnitudes of their Fourier transform," in *IEEE International Symposium on Information Theory*, 2012, pp. 1473–1477.

[12] P. Netrapalli, P. Jain, and S. Sanghavi, "Phase retrieval using alternating minimization," *IEEE Trans. Signal Process.*, vol. 63, no. 18, pp. 4814–4826, Sept. 2015.

[13] C. Qian, N. D. Sidiropoulos, K. Huang, L. Huang, and H. C. So, "Phase retrieval using feasible point pursuit: Algorithms and Cramer-Rao bound," *IEEE Trans. Signal Process.*, vol. 64, no. 20, pp. 5282–5296, Oct. 2016.

[14] G. Wang, G. B. Giannakis, J. Chen, and M. Akçakaya, "SPARTA: Sparse phase retrieval via truncated amplitude flow," in *IEEE Intl. Conf. Acoustics, Speech and Signal Process.*, New Orleans, USA, 2017.

[15] G. Wang, L. Zhang, G. B. Giannakis, J. Chen, and M. Akçakaya, "Sparse phase retrieval via truncated amplitude flow," *arXiv:1611.07641*, 2016.

[16] T. Bendory and Y. C. Eldar, "Non-convex phase retrieval from STFT measurements," *arXiv:1607.08218*, 2016.

[17] E. J. Candès, X. Li, and M. Soltanolkotabi, "Phase retrieval from coded diffraction patterns," *Appl. Comput. Harmon. Anal.*, vol. 39, no. 2, pp. 277–299, Sept. 2015.

[18] Y. Chen and E. J. Candès, "Solving random quadratic systems of equations is nearly as easy as solving linear systems," *Comm. Pure Appl. Math.*, 2016 (to appear).

[19] G. Wang, G. B. Giannakis, and Y. C. Eldar, "Solving systems of random quadratic equations via truncated amplitude flow," *arXiv:1605.08285*, 2016.

[20] R. Balan, P. Casazza, and D. Edidin, "On signal reconstruction without phase," *Appl. Comput. Harmon. Anal.*, vol. 20, no. 3, pp. 345–356, May 2006.

[21] A. Conca, D. Edidin, M. Hering, and C. Vinzant, "An algebraic characterization of injectivity in phase retrieval," *Appl. Comput. Harmon. Anal.*, vol. 38, no. 2, pp. 346–356, Mar. 2015.

[22] A. Ben-Tal and A. Nemirovski, *Lectures on Modern Convex Optimization: Analysis, Algorithms, and Engineering Applications.* SIAM, 2001, vol. 2.

[23] Y. Chen, X. Yi, and C. Caramanis, "A convex formulation for mixed regression with two components: Minimax optimal rates," in *Proc. of The 27th Conf. on Learn. Theory*, Paris, France, June 2014, pp. 560–604.

[24] K. G. Murty and S. N. Kabadi, "Some NP-complete problems in quadratic and nonlinear programming," *Math. Prog.*, vol. 39, no. 2, pp. 117–129, 1987.

[25] R. Ge, F. Huang, C. Jin, and Y. Yuan, "Escaping from saddle points–Online stochastic gradient for tensor decomposition," in *Proc. of 28th Conf. on Learn. Theory*, 2015, pp. 797–842.

[26] Y. N. Dauphin, R. Pascanu, C. Gulcehre, K. Cho, S. Ganguli, and Y. Bengio, "Identifying and attacking the saddle point problem in high-dimensional non-convex optimization," in *Adv. Neural Inf. Process. Syst.*, 2014, pp. 2933–2941.

[27] R. W. Gerchberg and W. O. Saxton, "A practical algorithm for the determination of phase from image and diffraction," *Optik*, vol. 35, pp. 237–246, Nov. 1972.

[28] I. Waldspurger, "Phase retrieval with random Gaussian sensing vectors by alternating projections," *aXiv:1609.03088*, 2016.

[29] C. Qian, X. Fu, N. D. Sidiropoulos, L. Huang, and J. Xie, "Inexact alternating optimization for phase retrieval in the presence of outliers," *arXiv:1605.00973v1*, 2016.

[30] G. Wang and G. B. Giannakis, "Solving random systems of quadratic equations via truncated generalized gradient flow," in *Adv. Neural Inf. Process. Syst.*, Barcelona, Spain, 2016.

[31] J. Sun, Q. Qu, and J. Wright, "A geometric analysis of phase retrieval," *arXiv:1602.06664*, 2016.

[32] T. Qiu, P. Babu, and D. P. Palomar, "PRIME: Phase retrieval via majorization-minimization," *IEEE Trans. Signal Process.*, vol. 64, no. 19, pp. 5174–5186, Oct. 2016.

[33] T. Qiu and D. Palomar, "Undersampled phase retrieval via majorization-minimization," *arXiv:1609.02842*, 2016.

[34] H. Zhang, Y. Chi, and Y. Liang, "Provable non-convex phase retrieval with outliers: Median truncated Wirtinger flow," *arXiv:1603.03805*, 2016.

[35] K. Wei, "Solving systems of phaseless equations via Kaczmarz methods: A proof of concept study," *Inverse Probl.*, vol. 31, no. 12, p. 125008, Nov. 2015.

[36] R. Kolte and S. A. Ozgur, "Phase retrieval via incremental truncated Wirtinger flow," *arXiv:1606.03196*, 2016.

[37] E. J. Candès, T. Strohmer, and V. Voroninski, "PhaseLift: Exact and stable signal recovery from magnitude measurements via convex programming," *Appl. Comput. Harmon. Anal.*, vol. 66, no. 8, pp. 1241–1274, Nov. 2013.

[38] I. Waldspurger, A. d'Aspremont, and S. Mallat, "Phase recovery, maxcut and complex semidefinite programming," *Math. Prog.*, vol. 149, no. 1-2, pp. 47–81, 2015.

[39] K. Huang, Y. C. Eldar, and N. D. Sidiropoulos, "Phase retrieval from 1D Fourier measurements: Convexity, uniqueness, and algorithms," *arXiv:1603.05215*, 2016.

[40] G. H. Golub and C. F. Van Loan, *Matrix Computations.* Johns Hopkins University Press, 2012, vol. 3.

[41] O. Shamir, "Fast stochastic algorithms for SVD and PCA: Convergence properties and convexity," in *The 33th Proc. of Intl. Conf. on Machine Learning*, New York City, NY, 2016.

[42] E. Oja, "Simplified neuron model as a principal component analyzer," *J. Math. Biol.*, vol. 15, no. 3, pp. 267–273, Nov. 1982.

[43] R. Johnson and T. Zhang, "Accelerating stochastic gradient descent using predictive variance reduction," in *Adv. Neural Inf. Process. Syst.*, 2013, pp. 315–323.

[44] S. Kaczmarz, "Angenherte auflsung von systemen linearer gleichungen," *Bulletin International de l'Acadmie Polonaise des Sciences et des Lettres. Classe des Sciences Mathmatiques et Naturelles. Srie A, Sciences Mathmatiques*, vol. 37, pp. 355–357, 1937.

[45] P. M. Pardalos and S. A. Vavasis, "Quadratic programming with one negative eigenvalue is NP-hard," *J. Global Optim.*, vol. 1, no. 1, pp. 15–22, 1991.

[46] D. K. Berberidis, V. Kekatos, G. Wang, and G. B. Giannakis, "Adaptive censoring for large-scale regressions," in *IEEE Intl. Conf. Acoustics, Speech and Signal Process.*, South Brisbane, QLD, Australia, 2015, pp. 5475–5479.

[47] G. Wang, D. Berberidis, V. Kekatos, and G. B. Giannakis, "Online reconstruction from big data via compressive censoring," in *IEEE Global Conf. Signal and Inf. Process.*, Atlanta, GA, 2014, pp. 326–330.

[48] J. Chen, G. Wang, and J. Sun, "Power scheduling for Kalman filtering over lossy wireless sensor networks," *IET Control Theory Appl.*, 2016 (to appear).

[49] R. Vershynin, "Introduction to the non-asymptotic analysis of random matrices," *arXiv:1011.3027*, 2010.

[50] T. Strohmer and R. Vershynin, "A randomized Kaczmarz algorithm with exponential convergence," *J. Fourier Anal. Appl.*, vol. 15, no. 2, pp. 262–278, 2009.
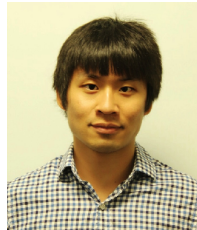
Gang Wang (S'12) received the B.Eng. degree in Electrical Engineering and Automation from Beijing Institute of Technology, Beijing, China, in 2011. He is currently working toward his Ph.D. degree in the ECE Dept. of the Univ. of Minnesota. His research interests focuses on the areas of high-dimensional structured signal processing, and (non)convex optimization for smart power grids.

Georgios B. Giannakis (F'97) received his Diploma in Electrical Engr. from the Ntl. Tech. Univ. of Athens, Greece, 1981. From 1982 to 1986 he was with the Univ. of Southern California (USC), where he received his MSc. in Electrical Engineering, 1983, MSc. in Mathematics, 1986, and Ph.D. in Electrical Engr., 1986. He was with the University of Virginia from 1987 to 1998, and since 1999 he has been a professor with the Univ. of Minnesota, where he holds an Endowed Chair in Wireless Telecommunications, a University of Minnesota McKnight Presidential Chair in ECE, and serves as director of the Digital Technology Center.

His general interests span the areas of communications, networking and statistical signal processing - subjects on which he has published more than 400 journal papers, 680 conference papers, 25 book chapters, two edited books and two research monographs (h-index 119). Current research focuses on learning from Big Data, wireless cognitive radios, and network science with applications to social, brain, and power networks with renewables. He is the (co-) inventor of 28 patents issued, and the (co-) recipient of 8 best paper awards from the IEEE Signal Processing (SP) and Communications Societies, including the G. Marconi Prize Paper Award in Wireless Communications. He also received Technical Achievement Awards from the SP Society (2000), from EURASIP (2005), a Young Faculty Teaching Award, the G. W. Taylor Award for Distinguished Research from the University of Minnesota, and the IEEE Fourier Technical Field Award (2015). He is a Fellow of EURASIP, and has served the IEEE in a number of posts, including that of a Distinguished Lecturer for the IEEE-SP Society.

Jie Chen received the B.S., M.S., and Ph.D. degrees from the Beijing Institute of Technology, Beijing, China, in 1986, 1996, and 2001, respectively. He is currently a professor with the School of Automation, Beijing Institute of Technology. His current research interests include complex systems, multi-agent systems, multi-objective optimization and decision, constrained nonlinear control, and optimization methods.